

Differences between  $\bar{p}p$  and  $pp$  interactions at 8.8 GeV/c and their relationship to  $\bar{p}p$  annihilations

C. N. Booth, R. E. Ansorge, J. R. Carter, W. W. Neale, J. G. Rushbrooke,  
A. J. Simmons, D. R. Ward, and T. O. White  
*Cavendish Laboratory, Cambridge, England*

R. A. Lewis, B. Y. Oh, M. Pratap,\* G. A. Smith, and J. Whitmore  
*Department of Physics, Michigan State University, East Lansing, Michigan 48824*

(Received 3 January 1983)

We report on an experiment in which the SLAC 40-in. hybrid facility was exposed to an 8.8-GeV/c antiproton beam. Using external detectors we have identified a large fraction of nonannihilation events and thus obtained a clean sample of annihilation data. Using proton interactions taken in the same detector at the same energy we have made a detailed study of  $(\bar{p}p - pp)$  differences and explored their relationship to  $\bar{p}p$  annihilations.

## I. INTRODUCTION

One topic of interest in the study of proton-antiproton interactions is the annihilation process,  $\bar{p}p \rightarrow$  mesons. Annihilations show a number of striking differences from  $\bar{p}p$  nonannihilations and other hadronic low- $p_T$  processes. For example, annihilations produce more particles on average, with higher transverse momentum, and show a comparative lack of leading particle effects. However, it is difficult to determine if these differences are caused by purely dynamical differences between the interaction mechanisms for annihilations and nonannihilations, since the presence of two baryons in the nonannihilation final state inevitably has kinematic effects on the distributions of the other produced particles. Data at higher energies may be expected to assist in this determination.

Almost all existing data on  $\bar{p}p$  annihilations, with the exception of exclusive final states such as  $\pi\pi$  or  $K\bar{K}$ , come from bubble-chamber experiments. At low energies a large fraction of the annihilation events can be identified through kinematic fitting. However, at high energies the cross sections for exclusive final states fall rapidly with increasing energy (typically like  $s^{-3}$ ), as one would expect for a baryon-exchange mechanism. Thus at high energies one is obliged to study "inclusive" annihilations. A number of methods may then be employed to isolate annihilation events:

(i) Kinematic fitting to exclusive channels. However, this becomes less effective as the energy increases.

(ii) Direct identification of the baryons and antibaryons in nonannihilations. However, in a bare

bubble chamber only about half of the protons and some hyperons can be identified at high energies.

(iii) Kinematic cuts based on the peripheral nature of baryon production; for example, events of the type  $\bar{p}p \rightarrow \bar{n}n + \pi$ 's will tend to have a larger missing mass than  $\bar{p}p \rightarrow \pi$ 's.

(iv) Subtraction of  $\bar{p}p$  and  $pp$  data. This method assumes that the differences between  $\bar{p}p$  and  $pp$  interactions are dominated by the  $\bar{p}p$  annihilation process. It is known, for example, that the difference between the  $\bar{p}p$  and  $pp$  total cross sections approximates the  $\bar{p}p$  annihilation cross section to  $\sim 10\%$  for beam energies up to  $\sim 10$  GeV.<sup>1</sup>

Existing data on inclusive  $\bar{p}p$  annihilations up to 12 GeV have used various combinations of methods (i), (ii), and (iii) above (e.g., Refs. 2 and 3) to separate annihilations from nonannihilations. Higher-energy experiments have relied entirely on method (iv) (e.g., Refs. 4 and 5) to estimate annihilation effects. For example, Fig. 1 shows a plot of the multiplicity correlation parameter  $f_2^{--}$  against the mean number of negative particles,  $\langle n_- \rangle$ , for  $\bar{p}p$  annihilations. Simple statistical models of annihilations can account for the linear fall of  $f_2^{--}$  with  $\langle n_- \rangle$  at low energies, but the higher-energy data indicate the onset of a new production mechanism, perhaps multiple cluster formation. However, the turn in the data just corresponds to the changeover in experimental technique to  $(\bar{p}p - pp)$  differences.

There is also theoretical interest in  $(\bar{p}p - pp)$  differences, particularly in the context of Regge theory. Particle-antiparticle differences are especially simple to describe in Regge theory, because many of the possible exchanges (including the poorly understood Pomeron) cancel out. For example, in the

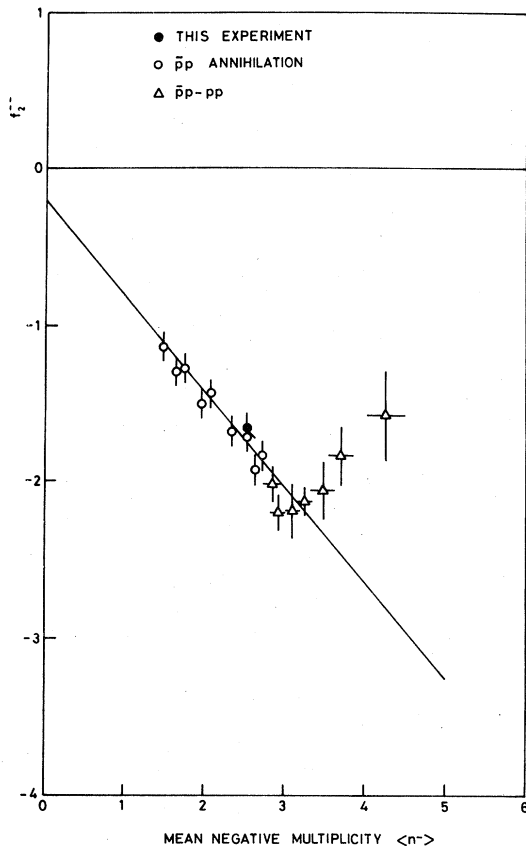


FIG. 1. The correlation moment for negative particles,  $f_{z^-}$ , plotted against  $\langle n_- \rangle$ , for  $\bar{p}p$  annihilations.

( $\bar{p}p - pp$ ) total-cross-section difference it is tempting to associate the  $\omega$ -exchange term (which takes the same sign in  $\bar{p}p$  and  $\bar{p}n$ ) with annihilations and the  $\rho$ -exchange term with nonannihilations. However, such a simple idea runs into problems when applied to other annihilation processes like  $\bar{\Omega}^+p$ . These ideas are reviewed in Ref. 6.

The data presented in this paper come from an experiment in which the SLAC 40-in. hybrid bubble chamber was exposed to 8.8-GeV/c antiproton and proton beams. The main aim of this experiment was to identify a large fraction of the  $\bar{p}$ 's and  $\bar{n}$ 's produced in the  $\bar{p}p$  nonannihilations. In this way we have been able to obtain a rather clean sample of annihilation events, mostly using method (ii) above. Furthermore, using the proton beam data we have been able to make a direct comparison of ( $\bar{p}p - pp$ ) differences with  $\bar{p}p$  annihilations with a minimum of systematic errors. Some preliminary results on this topic appear in Refs. 7 and 8, and other published results from this experiment may be found in Refs. 9–11.

The paper is outlined as follows. Section II de-

scribes the experimental procedure, and Sec. III explains the techniques used for separating annihilation and nonannihilation events. In Sec. IV, we give a comparison between ( $\bar{p}p - pp$ ) differences and  $\bar{p}p$  annihilations for various inclusive processes. We also study particle production in  $\bar{p}p$  annihilations and nonannihilations. Finally, in Sec. V, we make a brief comparison between our data and various quark-parton models.

## II. EXPERIMENTAL PROCEDURE

### A. The experiment

The experiment was performed at the SLAC hybrid facility (SHF),<sup>12</sup> which consisted of the 40-in. hydrogen bubble chamber with upstream multiwire proportional chambers (PWC's) and a Cherenkov counter to define the antiproton beam. Additional PWC's plus a large multicell Cherenkov counter (CANUTE) and matching hodoscope are used for downstream particle identification. Behind this, a calorimeter was placed to identify neutral particles. The apparatus and experimental procedures have been described in some detail in Ref. 10.

The chamber was exposed to a beam of momentum 8.8 GeV/c consisting of either antiprotons or protons, selected from other particles by an rf separator. The intensity was typically 1 or 2 particles per pulse. The bubble-chamber camera and flash tubes were under the control of a simple on-line trigger, which required that the beam particle had interacted within a suitable fiducial volume in the chamber. Data consisting of PWC hits and pulse heights from the Cherenkov, hodoscope, and scintillation counters of the calorimeter were recorded for each picture.

### B. Scanning and measurement of the film

The film was scanned for interactions of the triggered beam particle within the fiducial volume. Also recorded were slow protons, decays of neutral and charged particles and secondary interactions of neutral particles (principally antineutrons and neutrons) within the chamber. The scanning efficiency was determined by rescanning about  $\frac{1}{3}$  of the film. In all, 40 887  $\bar{p}p$  and 28 750  $pp$  events were found and measured. From some untriggered-bubble-chamber pictures, it was determined that some events were lost when the on-line trigger algorithm failed to detect the deflection of the beam particle. This occurred principally in elastic scatters, but also caused an asymmetry in the azimuthal distribution of forward tracks in inelastic events. The remaining events were weighted as a function of the vector

TABLE I. Event weighting.

Multiplicity	trigger	Weights to correct for losses due to		Overall weight
		scanning	measuring	
0	1.0	1.028	1.008	1.036
2 inel.	1.035	1.011	1.008	1.055
4	1.022	1.007	1.012	1.042
6	1.004	1.007	1.021	1.033
8	1.001	1.008	1.139	1.149
$\geq 10$	1.0	1.0	1.233	1.233
Overall	1.020	1.014	1.017	1.052

momentum of the tracks. The mean values of the weights are given, as a function of multiplicity, in Table I.

### C. Use of the external detectors

The external detectors were used in two ways—improvement of the momentum estimate and identification of particles. The use of the PWC planes to improve the momentum measurement obtained from the bubble chamber has already been described in detail in Refs. 10 and 11. CANUTE was used to identify many of the particles produced in the forward center-of-mass hemisphere. Protons and anti-protons produced no light, while pions above 1.5 GeV/c gave a signal in the counter. The threshold for charged kaons was 5.5 GeV/c. Since the probability of a secondary interaction in the bubble-chamber exit window or in the freon gas of CANUTE was not negligible, each track in the bubble chamber corresponding to a particle of momentum greater than 1.5 GeV/c was projected through the magnetic field to the Cherenkov-counter mirrors, and the PWC planes and hodoscope checked to ensure that the particle passed without secondary interaction. If no light was detected in the relevant CANUTE cell, the particle was tagged as an (anti) proton. If there was light, the radius of the spot produced by a pion of the appropriate momentum was calculated, and the pulse height from all cells covered by this spot were summed. Corrections were also made if the spot partially missed the edge of the counter. The particle was only identified as a pion if the pulse-height sum was consistent with that expected from a pion, if there was no overlap between the spots from different particles (a rare occurrence), and if no other particle showed signs of a secondary interaction, which could have contaminated the Cherenkov signature. The identification was also rejected if there were extra hits in the PWC's or hodoscope.

Fast neutrons and antineutrons were detected by showers induced in the calorimeter. Neutral parti-

cles were selected by the absence of a signal in the scintillator in front of the calorimeter. Hadrons were distinguished from photons by their different shower properties. The energy from an electromagnetic shower is deposited predominantly in the two  $\frac{1}{4}$ -in. lead plates placed in front of the calorimeter and the first few iron plates of the detector; hadronic showers are distributed through most of the iron-scintillator sandwich part of the calorimeter. The precise algorithm used to differentiate between the two shower types has been described in detail in Ref. 13. Once again,  $n/\bar{n}$  identification was only accepted if no charged particles had undergone a secondary interaction downstream. Using data on  $K_S^0$  decays in the chamber, we have estimated the  $K_L^0$  contamination of the  $n/\bar{n}$  showers, and find it negligible in general (see Sec. IV D). A small number of  $n/\bar{n}$  was also identified from interactions in the bubble chamber producing  $\geq 3$  charged particles.

Slow protons and pions in the momentum range 0.1–1.5 GeV/c were identified by visual inspection of the ionization in the bubble-chamber picture.

### D. Efficiency of particle identification

The four-constraint (4C) fitted events are known to be reliable<sup>10</sup> and can be used as a check on the efficiency and reliability of the charged particle identification. The identification of (anti) protons by CANUTE was found to be reliable above 3 GeV/c, with an efficiency increasing with momentum as shown in Fig. 2(a), due to both geometrical acceptance rising and the probability of secondary interactions falling. For slow protons, both the efficiency and reliability decreased with increasing momentum [Fig. 2(b)]. Below 1 GeV/c, both  $p$  and  $\pi$  identification were quite reliable, and proton identification could be used up to 1.5 GeV/c. From a knowledge of the observed spectra of  $p$ 's and  $\pi$ 's in any event sample, say of a given multiplicity, and the reliability and efficiency of the identification, the true  $p$  and  $\pi$  spectra could thus be determined

for momenta less than 1 GeV/c.

More care had to be taken with the use of one-constraint (1C) fits, where not all fits are correct. However, a sample of reliable 1C nonannihilation fits could be obtained<sup>13</sup> and used to check the  $\bar{n}$  detection efficiency in a way similar to that used for  $\bar{p}$  identification by CANUTE. The result is shown in Fig. 2(c), the efficiency being lower than that for  $\bar{p}$  because of the smaller acceptance. Spurious  $\bar{n}$  signals could arise from a number of sources—e.g., due to an undetected secondary interaction producing an  $\bar{n}$  or to an incorrect classification of shower type. The probability of a spurious signal was determined to be  $\sim 2\%$  by examining 4C or 1C events which did not contain an  $\bar{n}$ .

#### E. Separation of protons and pions

Many charged particles of momentum greater than 1 GeV/c could not be identified directly. Therefore a method was used to find the probability of each being a pion, as a function of momentum.<sup>14</sup> This was based on the charge-conjugation invariance of the  $\bar{p}p$  system and the symmetry of the  $pp$  state. When considered in the center-of-mass frame, the proton ( $\pi^+$ ) spectrum must be the reflection of that for antiprotons ( $\pi^-$ ). Thus, if positive particles are transformed to the center-of-mass frame, reflected and then transformed back to the laboratory frame, the spectrum of negative particles should be obtained. However, these transformations can only be done correctly if the appropriate mass is assumed for each positive particle. The probability of an ambiguous particle being a pion was parametrized as a function of longitudinal and transverse laboratory

momentum,  $\alpha(p_l, p_t)$ . The function  $\alpha$  was then determined by a least-squares fit to the data. Full details of the procedure are given in Ref. 15. The calculation was refined by subtracting from the ambiguous particles an estimate of the charged kaon contribution as determined from the  $K_S^0$  spectrum (see below).

#### F. Identification of neutral strange particles

Apart from  $n/\bar{n}$  detected in the calorimeter or by interaction in the chamber, the only way of identifying neutral particles was from their visible decays. All such decays ( $V$ 's) were measured and kinematic fits were attempted for the decays of  $K_S^0$ ,  $\Lambda$ , and  $\bar{\Lambda}$  and for photon conversion. In about 15% of the cases, more than one hypothesis gave a successful 3C fit to the  $V$ , the neutral particle being constrained to come from the primary vertex. Many of these ambiguities could be resolved by examining the ionization of the secondary tracks. Cuts on the decay transverse momentum and missing-mass rejected spurious fits to pair production. When remaining ambiguities had one fit with a  $\chi^2$  probability more than ten times greater than all others, this was accepted. Finally a few ambiguities between  $K_S^0$  and  $\Lambda$  and  $\bar{\Lambda}$  decays remained. These were resolved by plotting the cosine of the angle between the incoming neutral and outgoing negative particle against the Feynman  $x$  ( $p_l^*/p_{\max}^*$ ) of the neutral, for both unique and ambiguous cases. The identified  $K_S^0$  and  $\Lambda(\bar{\Lambda})$ 's mainly occupied different regions of the diagram, enabling the ambiguous cases to be allocated to one category or the other.<sup>15</sup>

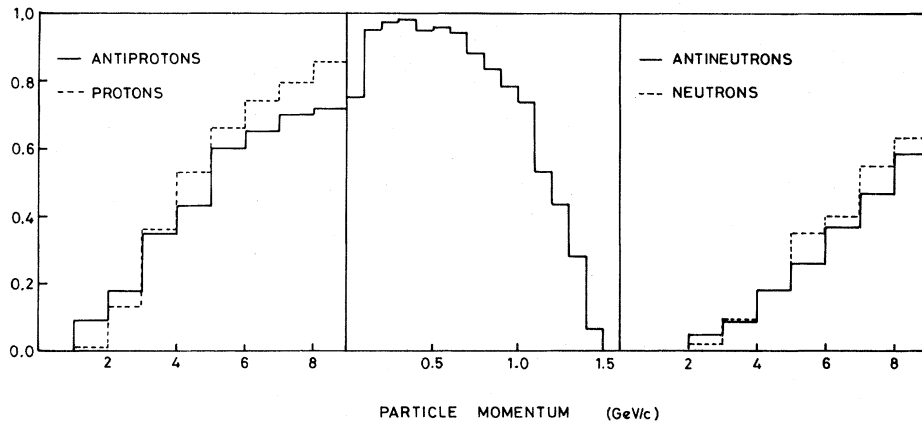


FIG. 2. (a) Detection efficiency of  $\bar{p}$  ( $p$ ) in  $\bar{p}p$  ( $pp$ ) interactions using CANUTE. (b) Detection efficiency of slow protons by ionization. (c) Detection efficiency of  $\bar{n}$  ( $n$ ) in  $\bar{p}p$  ( $pp$ ) interactions using the calorimeter.

### III. SEPARATION OF ANNIHILATION AND NONANNIHILATION EVENTS

Many nonannihilation interactions could be directly identified as such. However, others were not identifiable, and in order to extract a reasonably pure annihilation sample, it was necessary to do two things. First, the inefficiencies for baryon and antibaryon identification were used to correct the number of observed nonannihilations. These corrections were made for each multiplicity independently. In the examples given below, the case of four-prong events will be used. Unless otherwise stated, the same procedure was used for other multiplicities. Second, once the number of events in each category was known, kinematic cuts were chosen to separate the two classes as cleanly as possible. The  $pp$  data, taken under the same conditions and analyzed in an identical way, were an invaluable tool in this process.

#### A. Determination of number of nonannihilation events

Some events were identified directly as either nonannihilation or annihilation from the presence of a unique, reliable 4C or 1C kinematic fit. (In the case of ambiguous 1C fits, ionization scanning and CANUTE data were sometimes used to select the correct fit.) Other events were clearly identified as nonannihilations by the detection of a baryon or antibaryon. A number of events were recognized as due to annihilation because, no matter what particle assignments were made to the charged tracks, the missing mass was incompatible with the production of two baryons, either charged or neutral.

It was necessary to correct the observed nonannihilation events for the limited detected efficiency of, for example, antiprotons. Clearly, many events

with an undetected antiproton were still recognized as nonannihilation because the proton was identified, or the event was fitted, and it was important not to count these events twice. Table II shows the number of four-prong events with detected baryons or antibaryons which were not identified as annihilation or nonannihilation on the basis of a kinematic fit or missing mass. Events with an identified slow proton have been weighted by the probability that this identification was correct, as described in Sec. II.

A correction was made for undetected antiprotons. Using the momentum spectrum of observed antiprotons in events with no identified proton, together with the efficiency of CANUTE as a function of momentum, we could find the number of unseen antiprotons of momentum greater than 3 GeV/c (in events with no identified proton). (Below 3 GeV/c, the antiproton identification was not sufficiently reliable to be used.) The number of nonannihilations accounted for by this correction was 708 in  $\bar{p}p$  data (773 in  $pp$ ).

Before a similar correction could be applied for the  $\bar{n}$  detection efficiency, it was necessary to remove spurious  $\bar{n}$  signals. To correct for unobserved antineutrons (in events without an observed proton), an estimate of the  $\bar{n}$  detection efficiency was needed. This efficiency depended on the  $\bar{n}$ 's momentum. However, the calorimeter's energy resolution ( $\sim 150\%/\sqrt{E}$  for hadrons) was insufficient to determine a momentum spectrum. Various methods were used to estimate this spectrum, as described in Ref. 15, and eventually the antiproton spectrum (in events without identified protons) was used as an estimate. It was thus found that about 1400 nonannihilations were not recognized because of the loss of antineutrons in  $\bar{p}p$  events (and about 1100 through the loss of fast neutrons in  $pp$ ). The uncer-

TABLE II. Detection of baryons in unfitted four-prong events. In the  $pp$  case we call a baryon in the forward c.m. hemisphere a "fast" baryon, this corresponding approximately to the antibaryon in  $\bar{p}p$ .

	$\bar{p}p$			
	Antiproton	Antineutron	Antihyperon	No antibaryon
Proton	459	111	10	1124
Hyperon	16	5	3	68
No baryon	628	356	42	5177
	$pp$			
	Fast proton	Fast neutron	Fast hyperon	No fast baryon
Proton	419	185	21	1100
Hyperon	17	1	0	16
No baryon	851	256	36	2568

tainty in the  $\bar{n}$  spectrum contributes the largest part of the error in the overall nonannihilation cross section.

Some events were identified as nonannihilations by the detection of a  $\Lambda/\bar{\Lambda}$ . Again losses were present, due to neutral decay modes, decays outside the fiducial volume and other small effects such as scanning inefficiencies. A correction was made, taking due care over the production of  $\Lambda\bar{\Lambda}$  pairs, and  $\Lambda\bar{n}$  or  $\Lambda\bar{p}$ , where the  $\bar{n}$  or  $\bar{p}$ , though not observed, had been corrected for above. Thus double counting was avoided, and a correction to the nonannihilation sample for unseen hyperons of 52 events (45 for  $pp$ ) was made.

Ideally, after making all of the above corrections, every nonannihilation event should have been detected or corrected for. This was not so in practice as we can show for the  $pp$  data, where all events must be nonannihilations. After the above corrections 91.4% of the events were accounted for. The discrepancy arises from the limited detection of the small fraction of (anti)baryons produced with low forward momenta in the center-of-mass frame. (For example, a proton at rest in the center-of-mass had a laboratory momentum of about 2 GeV/c.) CANUTE identification of (anti)protons was unreliable, and so not used, below 3 GeV/c, and the (anti)neutron detection probability there was only a few per cent, rendering correction unreliable. Clearly, there must be similar events with rather slow antibaryons in the  $\bar{p}p$  data too, so it was assumed that the efficiency for counting nonannihilations, after all the above corrections had been applied, would be the same in the two sets of data. Thus the 8865 counted  $\bar{p}p$  nonannihilations should be 91.4% of the total, 9699 such interactions.

Two- and six-prong interactions were analyzed in exactly the same way as described for four-prong interactions. For higher multiplicities, where there were few nonannihilation events, the  $\bar{n}$  efficiency was low and could not be well determined. Therefore no attempt was made to correct for lost antineutrons, and the lower efficiency for counting nonannihilations determined from  $pp$  events was simply applied to the  $\bar{p}p$  data after correction for spurious  $\bar{n}$  signals and of the few antiprotons and hyperons present. For zero-prong events where the mean  $\bar{n}$  momentum was much higher than for other multiplicities (consequently, the calorimeter had a better energy resolution), it was possible to make a direct estimate of the  $\bar{n}$  momentum spectrum and detection efficiency. The calorimeter energy resolution was determined using a sample of 1C fits. A simple parametrization of the  $\bar{n}$  spectrum was folded in with this resolution and then fitted to the distribution of observed energy deposited in the calorime-

ter. For various parametrizations, the results were consistent with each other and also with the  $\bar{p}$  spectrum in inelastic two-prong events. This gave an estimate of the  $\bar{n}$  detection efficiency in zero-prong events of  $(36 \pm 2)\%$ . An adjustment was also made for the neutral decay mode,  $\bar{\Lambda} \rightarrow \bar{n}\pi^0$ , to avoid double counting in the corrections.

### B. Definition of the annihilation sample

As has been described, it was possible to find the number of nonannihilation and annihilation events in the data for each multiplicity. Just over 65% (47%) of the nonannihilation (annihilation) interactions were individually identified as such. It was necessary to classify the remaining events as accurately as possible. Nonannihilations might not be recognized either because a charged baryon and/or antibaryon was produced, but not recognized because of the limited efficiencies of ionization scanning and CANUTE, or because no charged baryon was produced and the  $\bar{n}$  was not detected. These two possibilities are discussed separately below.

In Sec. II, a method was outlined for finding the probability that an ambiguous particle was a pion or proton. If  $\beta_i$  is the probability that the particle  $i$  was a proton (or antiproton), we define a "nonannihilation function"  $Q$  which is a measure of the likelihood of the event containing a *charged* baryon:

$$Q = 1 - \prod (1 - \beta_i),$$

the product being over all tracks in the event. Clearly, events with a large value of  $Q$  are more likely to be nonannihilations, while those with low  $Q$  would be expected to be annihilations or to contain an  $n\bar{n}$  pair.

Nonannihilations with no charged baryons will have a larger missing mass than most annihilation events. The missing mass must be at least twice the neutron mass, but will usually be significantly higher as the neutron and antineutron are produced peripherally and tend to follow the initial proton and antiproton.

Figure 3 is a scatter plot of missing mass against  $Q$  for four-prong events which were not identified as either nonannihilation or annihilation. Annihilation interactions preferentially populate region A, of low missing mass and low  $Q$ . Nonannihilations with one or two charged baryons will be mainly in region B, while those with a neutral-baryon-antibaryon pair will be concentrated in area C at large missing mass and low  $Q$ . There is no clear separation, and to define an annihilation sample it was important to specify the cuts delimiting the regions correctly. This was done by a continuation of the calculations which found the number of annihilation events (and

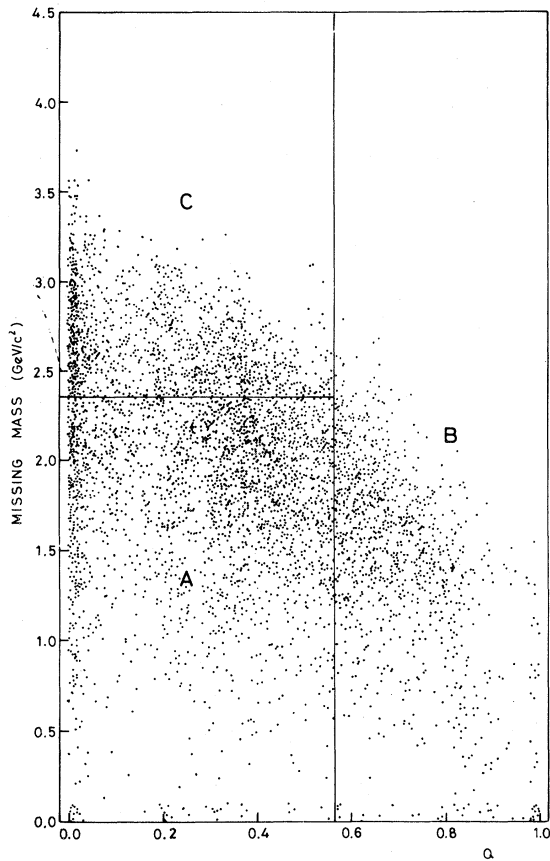


FIG. 3. Plot of missing mass against  $Q$  (the “nonannihilation” function defined in the text) for events ambiguous between annihilation or nonannihilation. Region A will mostly be populated by annihilations, while regions B and C will favor nonannihilations.

hence the number of events which should be in region A).

Just as corrections were made for the number of antiprotons and antineutrons in events *without* an identified proton, the same procedure was adopted for those events *with* such a particle. In this way, all antibaryons could be allocated in the nonannihilation sample as either  $\bar{p}$  or  $\bar{n}$  (the small numbers of  $\Lambda$ 's and  $\bar{\Lambda}$ 's being ignored in the following description). Thus we arrive at the data Table III(a) with antibaryons accounted for, but still having uncertainties in the distribution of protons and neutrons in the baryon column. In this table, fitted events are once more included. The value of the  $\bar{p}:\bar{n}$  ratio (0.72:0.28) provides a valuable check at this stage, as the number of protons was also determined independently from the proton/pion separation described in Sec. II. This yielded a  $p:n$  ratio of 0.68:0.32. For two-, four-, and six-prong data, the ratios are in agreement, within errors, for the two methods.

To find the fraction of nonannihilations with no charged baryons, it was necessary to resolve the ambiguities of Table III(a). Charge-conjugation symmetry implies that the number of “ $\bar{n}p$ ” events must equal that of the “ $\bar{p}n$ ” events, just as the total number of protons must be the same as that of antiprotons. This input, together with the assumption that the unidentified protons were in “ $\bar{p}p$ ” and “ $\bar{n}p$ ” in the same ratio as the identified protons (for unfitted events) enabled the assignment of events given in Table III(b). Further details of these calculations can be found in Ref. 15. We now have the necessary information to find the breakdown of baryons and antibaryons in the *unidentified* nonannihilations and

TABLE III. Baryons and antibaryons in four-prong nonannihilations.

(a) After correcting for antibaryon detection efficiencies	
$\bar{p}p$	4331
$\bar{n}p$	846
$\bar{p}n$	522
$\bar{p}?$	1860
$\bar{n}?$	1743
(b) After determination of unseen protons	
$\bar{p}p$	5521
$\bar{n}p$	1192
$\bar{p}n$	1192
$\bar{n}n$	1396
(c) Baryons and antibaryons in four-prong unidentified nonannihilations	
$\bar{p}p$	788
$\bar{n}p$	278
$\bar{p}n$	442
$\bar{n}n$	1113

this is given in Table III(c). Thus the cuts to define the regions of Fig. 3 are determined: region A contains the number of unidentified annihilation events, C contains the number of unidentified " $\bar{n}n$ " events and the remainder, B, is the number of nonannihilations with an unidentified baryon and/or antibaryon.

The reliability of this separation into annihilations and nonannihilations is of great importance to many of the results presented in this paper. A number of tests, for example, of charge conjugation of final samples, were applied and showed no significant inconsistencies. In fact, the properties of the samples were not significantly altered if the cuts were changed slightly, changing the number of events in B and C by up to 10% of the number of annihilations, while keeping the number in A constant.

A Monte Carlo program was also used to investigate the separation method. Antiproton-proton interactions were simulated using an event generator which produced interactions according to phase space with a limited transverse momentum. Leading baryons and diffractive events were included for nonannihilations. The experimentally determined particle identification efficiencies were used to simulate detection of baryons and antibaryons. Approximately the observed fraction of nonannihilations were predicted to be recognized. For the ambiguous events, a plot of missing mass against  $Q$  was made, and for each multiplicity found to be similar to the plot produced from the experimental data. It was found that the experimentally determined cuts on  $Q$  and missing mass were close to the best place to separate the two types of interactions in the computer-generated events. By observing the overlap of points from the two types of interactions, the Monte Carlo also enabled an estimate to be made of the contamination in the so-called annihilation and nonannihilations. The purity of the samples is in the range 70–90%, as given in Table IV. It is greatest for two-prong nonannihilations and six-prong annihilations where the other component of the cross sections is relatively small.

#### IV. $\bar{p}p$ ANNIHILATIONS AND ( $\bar{p}p - pp$ ) DIFFERENCES

In this section we present our results on inclusive  $\bar{p}p$  annihilations and compare the annihilation data both with  $\bar{p}p$  nonannihilations and with the estimates of  $\bar{p}p$  annihilations using ( $\bar{p}p - pp$ ) differences.

##### A. Topological cross sections

A number of corrections were needed to obtain cross sections for the production of different num-

TABLE IV. Purity of the annihilation and nonannihilation samples (based on Monte Carlo calculations).

Charged multiplicity	Purity of nonannihilations	Purity of annihilations
2	97%	68%
4	92%	82%
6	78%	90%

bers of charged particles. Scanning and measuring efficiencies were determined separately for each charged multiplicity. The two-prong events were separated into elastic and inelastic categories by kinematic fits. There was a substantial loss of low-momentum-transfer-squared ( $t$ ) elastic scatters, caused partly by scanning losses and partly by the on-line trigger algorithm. These losses were estimated by fitting those elastics with  $0.15 < |t| < 0.4$  GeV<sup>2</sup> to an exponential form. The trigger also caused a loss of  $\sim 2\%$  of inelastic events in which a secondary particle faked an undeflected beam particle and a weight was applied to each event to correct for this. Corrections were also made for undetected Dalitz pairs and for  $\gamma$  conversions or neutral-strange-particle decays close to the interaction point. These corrections were based on the cross sections given in Secs. IV C and IV D.

The data were normalized to total cross sections derived by interpolating the results obtained in a number of other experiments.<sup>16</sup> The topological cross sections so calculated are given in Table V. The errors are purely statistical, except in the two-prong case, where the uncertainties in the elastic/inelastic separation are reflected in the errors.

The annihilation and nonannihilation cross sections are also given in Table V, together with some of the lower moments of the multiplicity distribution. We note two of the well-known differences between  $\bar{p}p$  annihilations and nonannihilations:  $\langle n \rangle$  is higher by about two units in annihilations and the multiplicity distribution is narrower in proportion to its mean (i.e.,  $\langle n \rangle / D$  is greater).

The conjecture that  $\bar{p}p$  annihilations may be equated with ( $\bar{p}p - pp$ ) differences is equivalent to assuming the equality of  $\bar{p}p$  nonannihilations and  $pp$  interactions. Data on exclusive nonannihilation channels (e.g., comparing  $\bar{p}p\pi^+\pi^-$  with  $pp\pi^+\pi^-$  final states) suggest that this relation holds better for higher multiplicities,<sup>10</sup> and becomes more reliable as the interaction energy increases.<sup>8</sup> The data of Table V show significant discrepancies between  $\bar{p}p$  nonannihilations and  $pp$  interactions in zero- and two-

TABLE V. Topological cross sections and moments in  $\bar{p}p$  and  $pp$  interactions at 8.8 GeV/c. In the columns headed  $pp$ ,  $\bar{p}p$ , and  $(\bar{p}p - pp)$  the errors are statistical only, except for the two-prong events where systematic errors arising from the separation of elastics and inelastics are allowed for. Uncertainties in normalization (caused by errors in  $\sigma_{\text{tot}}$ ) are not included. In the  $\bar{p}p$  annihilation and non-annihilation data systematic errors in the separation procedures are included. Similar comments apply to succeeding tables.

Charged multiplicity	Cross sections (mb)				
	$pp$	$\bar{p}p$	$\bar{p}p$ Nonannihilation	$\bar{p}p$ Annihilation	$(\bar{p}p - pp)$
0		2.35 $\pm$ 0.06	2.22 $\pm$ 0.11	0.13 $\pm$ 0.11	2.35 $\pm$ 0.06
2 (elastic)	9.80 $\pm$ 0.30	12.33 $\pm$ 0.40			
2 (inelastic)	15.46 $\pm$ 0.30	14.63 $\pm$ 0.30	13.04 $\pm$ 0.37	1.59 $\pm$ 0.26	-0.83 $\pm$ 0.42
4	12.53 $\pm$ 0.18	16.79 $\pm$ 0.21	12.08 $\pm$ 0.35	4.70 $\pm$ 0.33	4.26 $\pm$ 0.28
6	2.06 $\pm$ 0.05	7.68 $\pm$ 0.12	2.31 $\pm$ 0.20	5.37 $\pm$ 0.22	5.62 $\pm$ 0.13
8	0.10 $\pm$ 0.01	1.86 $\pm$ 0.05	0.09 $\pm$ 0.03	1.78 $\pm$ 0.06	1.76 $\pm$ 0.05
10	0.001 $\pm$ 0.001	0.23 $\pm$ 0.02	0.002 $\pm$ 0.001	0.23 $\pm$ 0.02	0.23 $\pm$ 0.02
12		0.017 $\pm$ 0.005		0.017 $\pm$ 0.005	0.017 $\pm$ 0.005
All inelastic	30.17 $\pm$ 0.30	43.57 $\pm$ 0.40	29.74 $\pm$ 0.55	13.83 $\pm$ 0.49	13.40 $\pm$ 0.50
Total (input value)	39.97 $\pm$ 0.3	55.90 $\pm$ 1.5			15.93 $\pm$ 1.5
Moments					
$\langle n \rangle$	3.12 $\pm$ 0.02	3.67 $\pm$ 0.02	2.98 $\pm$ 0.03	5.11 $\pm$ 0.08	4.90 $\pm$ 0.10
$D = (\langle n^2 \rangle - \langle n \rangle^2)^{1/2}$	1.27 $\pm$ 0.01	1.92 $\pm$ 0.01	1.52 $\pm$ 0.02	1.89 $\pm$ 0.06	2.50 $\pm$ 0.03
$f_2 = \langle n(n-1) \rangle - \langle n \rangle^2$	-1.51 $\pm$ 0.02	0.03 $\pm$ 0.03	-0.67 $\pm$ 0.05	-1.55 $\pm$ 0.27	1.33 $\pm$ 0.22
$\langle n_- \rangle$	0.56 $\pm$ 0.01	1.84 $\pm$ 0.01	1.49 $\pm$ 0.02	2.55 $\pm$ 0.04	2.45 $\pm$ 0.05
$f_2^-$	-0.16 $\pm$ 0.05	-0.91 $\pm$ 0.08	-0.91 $\pm$ 0.02	-1.66 $\pm$ 0.08	-0.89 $\pm$ 0.06

prong events, but for higher multiplicities the data are consistent with being equal, though we cannot exclude discrepancies at the 10% level.

The subtraction method is clearly wrong for the zero- and two-prong events. For the zero-prong events the  $(\bar{p}p - pp)$  difference is dominated by nonannihilation processes (of the kind  $\bar{p}p \rightarrow \bar{n}n + \pi^0$ 's), while the two-prong difference is negative. However, if the zero- and two-prong events are added together, then the subtraction method gives a satisfactory result; this seems to work quite well in other contexts also, as will appear below. For multiplicities 4 and above the annihilation and difference data are consistent with being equal, though there could be discrepancies of  $\sim 5-10\%$  in the four- and six-prong events. Thus, since we have noted that discrepancies between exclusive reactions in  $\bar{p}p$  and  $pp$  grow smaller as the energy increases, we may feel some confidence in the subtraction technique at higher energies, despite the falling annihilation/nonannihilation ratio.

It is clear, though, that the subtraction method cannot be used naively in the lower-multiplicity channels. Two specific procedures have been proposed to overcome this problem. Rushbrooke *et al.*<sup>4</sup> have taken the zero-prong annihilation cross section to be zero, used a power-law extrapolation of low-

energy data for the two-prong events and employed simple differences for high multiplicities. D'Innocenzo *et al.*<sup>17</sup> have proposed an alternative method, whereby the  $n$ -prong  $\bar{p}p$  nonannihilation (nondiffractive) cross section is given by  $(1-\delta)\sigma_n(pp) + \delta\sigma_{n+2}(pp)$ . In effect, a constant fraction  $\delta$ , of the  $pp$  cross section is shifted down in multiplicity. In Table VI, we compare our annihilation data with these "corrected difference" algorithms, using  $\delta=0.12$  (from a fit to data using the procedure of Ref. 17) in the second method. It is clear that either technique is preferable to the "naive subtraction" method. Probably the Rushbrooke procedure gives slightly better results, though the D'Innocenzo method is better in the two-prong case.

Our annihilation cross sections may be compared with those of Ref. 2 at a very similar momentum, 9.1 GeV/c. The data appear to agree well except in the two-prong events, where we find a significantly higher cross section. Also Ref. 2 quotes no zero-prong annihilation value. There is, however, a normalization discrepancy, since Ref. 2 finds a total annihilation cross section into pions of  $13.2 \pm 0.5$  mb, while our value,  $13.83 \pm 0.49$  mb includes kaonic annihilations ( $\sim 2.5$  mb, see Sec. IV D). This disagreement is partly caused by different total cross sections used for normalizations; it is also possible that

TABLE VI. Comparison of difference methods for topological cross sections.

Charged multiplicity	Annihilation data	Naive subtraction	Rushbrooke method (Ref. 4)	D'Innocenzo method (Ref. 17)
0	0.13±0.11	2.35±0.06	0	0.96±0.21
2	1.54±0.29	-0.83±0.42	1.20±0.20	1.77±0.78
4	4.70±0.33	4.26±0.28	4.26±0.28	5.35±0.37
6	5.37±0.22	5.62±0.13	5.62±0.13	5.84±0.15
8	1.78±0.06	1.76±0.05	1.78±0.05	1.77±0.05
≥ 10	0.25±0.02	0.25±0.02	0.25±0.02	0.25±0.02
Total	13.83±0.49	13.40±0.50	13.11±0.37	15.94±0.90
$\langle n \rangle$	5.11±0.08	4.90±0.10	5.33±0.06	4.82±0.15

a small number of charged kaons are misidentified as  $p$  or  $\bar{p}$  in our experiment.

A question of long-standing interest is whether the annihilation cross section equals the difference between  $\bar{p}p$  and  $pp$  total cross sections. Our data in Table V tend to indicate that the difference in inelastic cross sections is a more appropriate choice. However, models involving absorption effects favor an annihilation cross section greater than the  $(\bar{p}p - pp)$  difference,<sup>6</sup> because a final-state interaction in a  $\bar{p}p$  nonannihilation reaction could give rise to an annihilation final state. It is clear from the results of Table V that such effects must be small at this energy.

### B. Charged-pion production

We have noted that  $\bar{p}p$  nonannihilations have a lower  $\langle n \rangle$  than  $pp$  interactions. This is not surprising in view of the possibility of charge annihilation in the  $\bar{p}p$  case; indeed a similar difference is seen between  $\pi^-p$  and  $\pi^+p$  interactions.<sup>18</sup> Also the  $\bar{p}p$  annihilation cross section is a little lower than  $pp$ , and therefore simple  $(\bar{p}p - pp)$  differences underestimate the cross section for charged-particle production in  $\bar{p}p$  annihilations by  $\sim 10\%$ .

However, this discrepancy in charged-particle production between  $\bar{p}p$  nonannihilations and  $pp$  can

be entirely accounted for in terms of the different production of charged baryons and antibaryons. This is demonstrated in Table VII on charged-particle and  $p/\bar{p}$  production (based on the  $p/\pi$  separation procedure outlined in Sec. II). For each multiplicity the difference in charged particle production and in baryon/antibaryon production is consistent with being equal. In other words, the effect of the different charges of the beam particles is largely reflected in the leading particles produced, i.e., the baryons and antibaryons.

We may therefore expect that  $\pi^\pm$  cross sections in  $\bar{p}p$  annihilations should be well approximated by  $(\bar{p}p - pp)$  differences of  $\pi^\pm$  cross sections. This is borne out by the data presented in Table VIII. The  $(\bar{p}p - pp)$  cross sections are consistent with the annihilations in all multiplicities, and agree overall to better than 2%. However, one would not expect the subtraction method to work for  $\pi^+$  and  $\pi^-$  separately, since in  $\bar{p}p$  the  $\pi^+$  and  $\pi^-$  cross sections must be equal by  $C$  invariance, whereas in  $pp$  from charge conservation cross sections for  $\pi^+$  and  $\pi^-$  could only be equal if precisely two protons were produced per event, which is clearly not the case (Table VII).

Nevertheless, one might still hope to use the  $(\bar{p}p - pp)$  subtraction method for  $\pi^+$  and  $\pi^-$  production separately in certain regions of phase space, for example in the beam and target fragmentation

TABLE VII. Cross sections for charged-particle production and for  $p/\bar{p}$  production (in mb).

Charged multiplicity	$pp \rightarrow$ all charged	$\bar{p}p$ (Nonann) $\rightarrow$ all charged	$pp \rightarrow p + X$	$\bar{p}p \rightarrow p/\bar{p} + X$
2	30.9±0.6	26.1±0.7	16.0±0.3	11.6±0.2
4	50.1±0.7	48.3±1.4	18.3±0.3	16.8±0.2
6	12.4±0.3	13.9±1.2	3.4±0.1	3.1±0.2
8	0.8±0.1	0.7±0.2	0.16±0.04	0.12±0.12
Total	94.2±1.0	89.0±2.0	37.5±0.4	31.4±0.6

TABLE VIII. Cross sections for  $\pi^\pm$  production (in mb).

Charged multiplicity	$pp$	$\bar{p}p$	$\bar{p}p$ nonannihilation	$\bar{p}p$ annihilation	$(\bar{p}p - pp)$
2	$14.7 \pm 0.3$	$16.2 \pm 0.4$	$14.0 \pm 0.4$	$2.2 \pm 0.4$	$1.5 \pm 0.5$
4	$31.9 \pm 0.5$	$48.2 \pm 0.6$	$30.4 \pm 0.9$	$17.8 \pm 1.2$	$16.3 \pm 0.8$
6	$9.2 \pm 0.3$	$41.8 \pm 0.6$	$10.2 \pm 0.9$	$31.6 \pm 1.2$	$32.6 \pm 0.7$
8	$0.62 \pm 0.09$	$14.7 \pm 0.6$	$0.52 \pm 0.40$	$14.2 \pm 0.4$	$14.1 \pm 0.6$
10	$0.02 \pm 0.02$	$2.4 \pm 0.2$	$0.06 \pm 0.03$	$2.4 \pm 0.2$	$2.4 \pm 0.2$
12				$0.20 \pm 0.06$	$0.20 \pm 0.06$
Total	$56.4 \pm 0.6$	$123.6 \pm 1.2$	$55.2 \pm 1.2$	$68.4 \pm 2.4$	$67.2 \pm 1.3$

regions. In Fig. 4, we show the cross sections for  $\pi^+$  and  $\pi^-$  production in  $pp$  and  $\bar{p}p$  interactions as a function of Feynman  $x$ ,  $p_l^*/p_{\max}^*$ . The  $\bar{p}p$  data are shown for the total sample and for the annihilation and nonannihilation events separately. Here and subsequently we have used the symmetry properties of the  $pp$  and  $\bar{p}p$  systems, averaging the forward and backward c.m. hemispheres in  $pp$ , and averaging forward  $\pi^\pm$  with backward  $\pi^\mp$  in  $\bar{p}p$ . Figure 5 shows

the corresponding plots for the c.m. rapidity variable  $y^* = \frac{1}{2} \ln[(E^* + p_l^*)/(E^* - p_l^*)]$ , and Fig. 6 contains the  $\pi^\pm$  cross sections as a function of transverse momentum squared,  $p_T^2$ .

Using these data we have investigated the  $(\bar{p}p - pp)$  subtraction technique in different kinematic regions. In Fig. 7, we show the ratio of the  $(\bar{p}p - pp)$  difference cross section to the  $\bar{p}p$  annihilation value. The data are shown for  $\pi^+$  and  $\pi^-$  separately and for  $\pi^\pm$  combined, as a function of  $x$ ,  $y^*$ , and  $p_T$ . The two longitudinal variables,  $x$  and

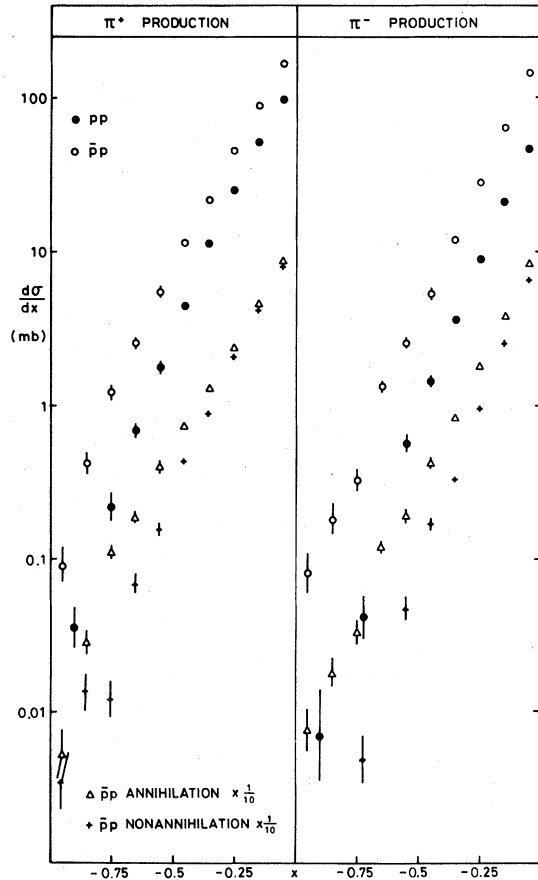


FIG. 4.  $d\sigma/dx$  for  $\pi^+$  and  $\pi^-$  production in the backward c.m. hemisphere. For clarity the  $\bar{p}p$  annihilation and nonannihilation data are scaled down by  $\frac{1}{10}$ .

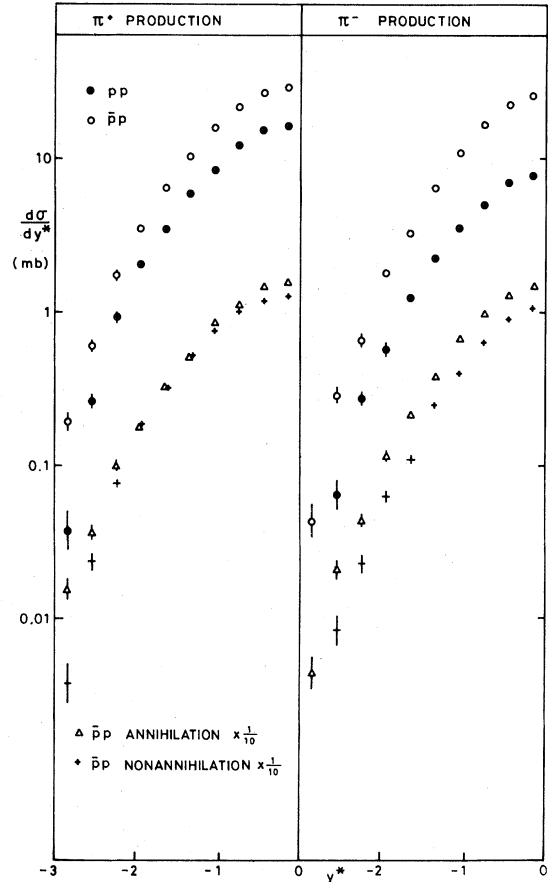


FIG. 5. As Fig. 4, showing  $d\sigma/dy^*$ .

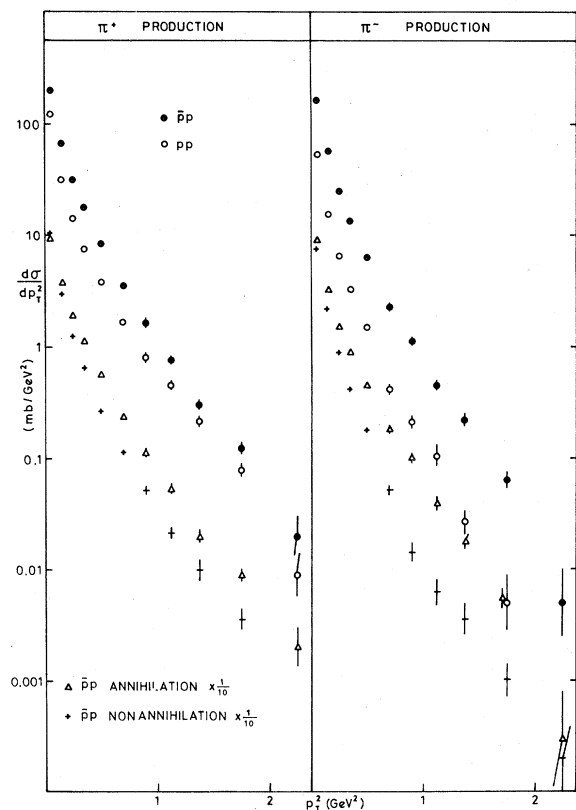


FIG. 6. As Fig. 4, showing  $d\sigma/dp_T^2$  (in the backward c.m. hemisphere).

$y^*$ , show much the same effects. In the proton fragmentation region the subtraction works quite well for both  $\pi^+$  and  $\pi^-$ ; there appear to be small systematic discrepancies with  $(\bar{p}p - pp)$  differences overestimating  $\pi^-$  production by  $\sim 5-10\%$ , and underestimating  $\pi^+$  by a similar amount. However, in the central region, near  $x = y^* = 0$ , the discrepancies rise to  $\sim 20\%$ . If  $\pi^+$  and  $\pi^-$  are combined, though, the  $(\bar{p}p - pp)$  difference technique gives a very good description of the annihilation data at all  $x$  and  $y^*$ . A similar conclusion applies to the  $p_T$  distribution, though it is possible that the subtraction method underestimates the annihilations at higher  $p_T$  values,  $\geq 1$  GeV/c.

These findings may be compared with the predictions of Mueller-Regge theory. The authors of Ref. 6 have shown that if the  $\omega$ -exchange term is really associated with annihilations, then annihilations should comprise  $\sim 75\%$  of the  $(\bar{p}p - pp)$  difference in the fragmentation region. In fact, the subtraction method works rather better than this, even though our experiment is at too low an energy to apply Regge theory reliably. In the central region Mueller-Regge theory requires that  $\pi^+$  and  $\pi^-$  be combined in order to obtain the correct energy dependence, and that then the  $(\bar{p}p - pp)$  difference should be at least 95% annihilations. Our data are clearly consistent with this conclusion.

It is obvious that the  $(\bar{p}p - pp)$  differences cannot work for  $\pi^+$  and  $\pi^-$  separately at all values of  $x$ , be-

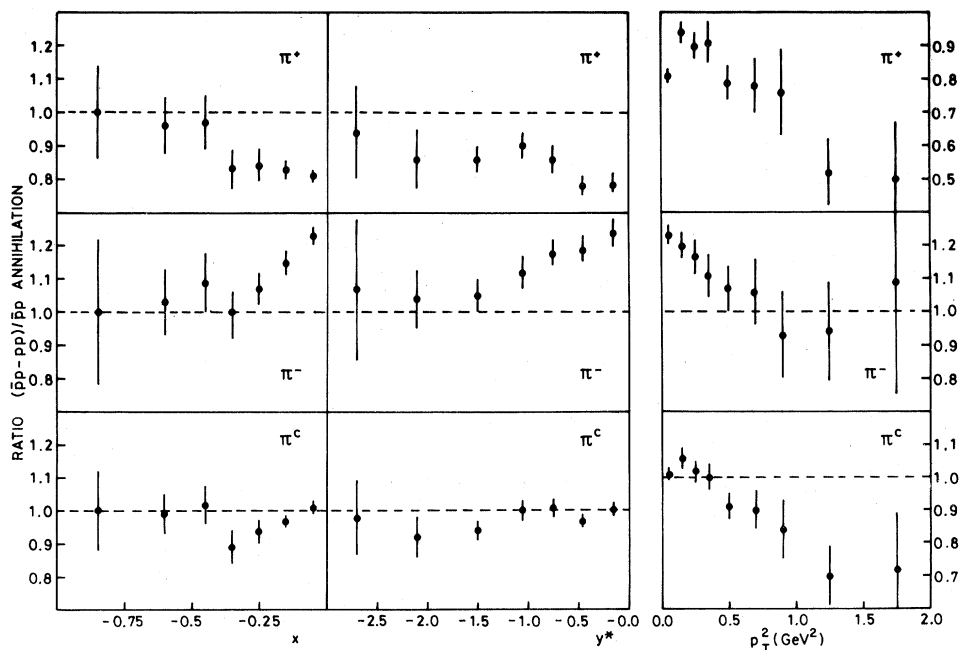


FIG. 7. Ratio of  $(\bar{p}p - pp)$  differences to  $\bar{p}p$  annihilations for  $\pi^+$ ,  $\pi^-$ , and  $\pi^c$  production as a function of  $x$ ,  $y^*$ , and  $p_T^2$  in the backward c.m. hemisphere.

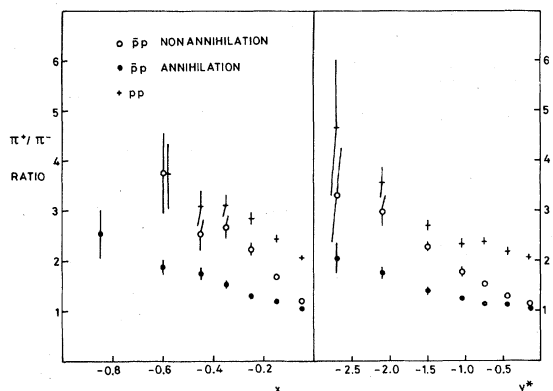


FIG. 8. Ratio of  $\pi^+$  to  $\pi^-$  as a function of  $x$  and  $y^*$  for  $pp$  interactions,  $\bar{p}p$  annihilations and  $\bar{p}p$  nonannihilations.

cause of the different symmetry properties of the  $pp$  and  $\bar{p}p$  systems. A solution to this problem has been suggested in Ref. 19, effectively based on two assumptions. Firstly, the  $(\bar{p}p - pp)$  method is assumed to be correct for  $\pi^\pm$  combined; we have seen that this is justified. Secondly, the  $\pi^+/\pi^-$  ratio is assumed to be the same in annihilations and nonannihilations. This ratio is plotted in Fig. 8. We see a significant difference between  $\bar{p}p$  annihilations and nonannihilations, the  $\pi^+/\pi^-$  ratio being greater in the latter case. We shall return to this point in Sec. V.

In Fig. 9, we make some further comparisons between  $\bar{p}p$  annihilations and nonannihilations. We plot the annihilation/nonannihilation ratio as a function of  $x$ ,  $y^*$ , and  $p_T$  for  $\pi^+$ ,  $\pi^-$ , and  $\pi^\pm$ . The annihilation events clearly show broader  $x$  and  $y^*$  distributions. This could be in some degree a kinematic effect, caused by the absence of leading baryons in the annihilation case. The  $p_T$  distribution shows a far more striking effect, with a rapid rise in the ratio as  $p_T$  increases. Table IX gives values of the mean transverse momentum  $\langle p_T \rangle$ ; and we see that  $\langle p_T \rangle$  is higher in annihilations by  $\sim 45$  MeV/c. However, even here kinematic effects may be present. The value of  $\langle p_T \rangle$  is known to increase with  $|x|$ , so is the broader  $x$  distribution leading to a higher  $\langle p_T \rangle$  in annihilations? Figure 10 shows that  $\langle p_T \rangle$  is in fact higher in annihilations at all values of  $x$ , except for  $|x| > 0.7$ . Also, the need to retain two baryons in the nonannihilation events effectively reduces the phase-space available for pion production. It might be more appropriate to compare  $\langle p_T \rangle$  in annihilations with nonannihilations at a higher energy at which roughly the same number of pions is produced, i.e., around 100 GeV/c in our case. At this energy  $\langle p_T \rangle$  is  $\sim 0.34$  GeV/c for pion production,<sup>15,20</sup> not very different from our annihilation value. It is therefore not clear whether the high  $\langle p_T \rangle$ 's seen in some low-multiplicity annihilation channels<sup>21</sup> are really typical of annihilations.

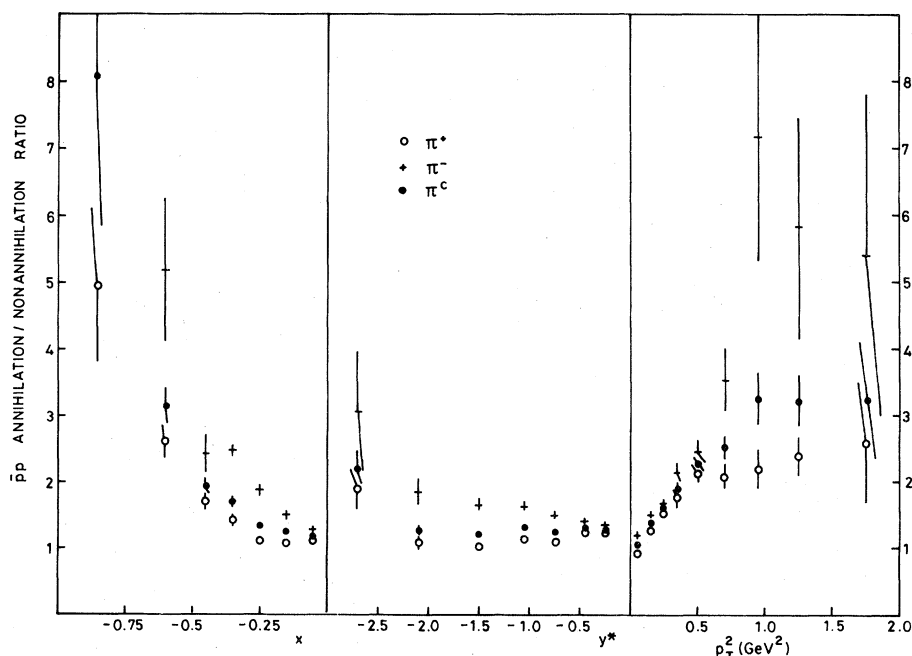


FIG. 9. Ratio of  $\bar{p}p$  annihilations to nonannihilations for  $\pi^+$ ,  $\pi^-$ , and  $\pi^0$  production as a function of  $x$ ,  $y^*$ , and  $p_T^2$  in the backward c.m. hemisphere.

TABLE IX. Average transverse momenta (in GeV/c) for the production of various particle species.

Particle type	$pp$	$\bar{p}p$	$\bar{p}p$ nonannihilation	$\bar{p}p$ annihilation
$\pi^+$ (backward c.m. hemisphere)	$0.299 \pm 0.002$	$0.333 \pm 0.001$	$0.307 \pm 0.002$	$0.356 \pm 0.002$
$\pi^-$ (backward c.m. hemisphere)	$0.288 \pm 0.002$	$0.321 \pm 0.001$	$0.289 \pm 0.002$	$0.343 \pm 0.002$
$p/\bar{p}$	$0.412 \pm 0.002$	$0.394 \pm 0.003$	$0.394 \pm 0.003$	
$\gamma$	$0.161 \pm 0.005$	$0.172 \pm 0.003$	$0.161 \pm 0.005$	$0.183 \pm 0.005$
$K_S^0$	$0.375 \pm 0.014$	$0.383 \pm 0.008$	$0.378 \pm 0.018$	$0.388 \pm 0.010$
$\Lambda/\bar{\Lambda}$	$0.436 \pm 0.013$	$0.427 \pm 0.008$	$0.427 \pm 0.008$	

### C. Photon production

The conversions of  $\gamma$  rays were separated from  $K_S^0$  and  $\Lambda^0$  decays by means of kinematic fits and cuts, as described in Sec. II F. The data were corrected for scanning and measuring efficiencies, and for losses of  $\gamma$ 's converting outside a fiducial volume, or closer than 1 cm to their production point. The pair-production cross sections of Ref. 22 were used for this purpose. However, even with these corrections there appeared to be losses of  $\gamma$  rays of energy  $< 120$  MeV in the laboratory. We attribute this partly to the falling cross section for pair production, and partly to problems in measuring tightly spiraling  $e^+$  and  $e^-$  tracks accurately. Therefore, we have rejected all photons below 120 MeV in the backward c.m. hemisphere, and doubled the weights of those which have laboratory energies  $< 120$  MeV after reflection about  $x = 0$  in the c.m. system.

In Table X, we give cross sections for  $\gamma$  production in  $pp$  and  $\bar{p}p$  nonannihilation and annihilation reactions. A small extra correction was required in

the  $\bar{p}p$  case, because of the missing mass cut used in the final separation of annihilations and nonannihilations. This cut could tend to class annihilations with large numbers of unseen  $\gamma$  rays as nonannihilations. Corrections were made using a cylindrical-phase-space Monte Carlo,<sup>23</sup> but were only significant in the case of six-prong events.

The data show that the overall annihilation cross section for  $\gamma$  rays is in reasonable agreement with the  $(\bar{p}p - pp)$  difference. The main contribution to  $\gamma$ -ray production is probably  $\pi^0$  decays, and one might expect the subtraction technique to work better than for  $\pi^+$  and  $\pi^-$ , because the  $\pi^0$  is an eigenstate of charge conjugation like the  $\bar{p}p$  system, whereas it is only if  $\pi^+$  and  $\pi^-$  are combined that they can be charge-conjugation eigenstates. The subtraction method also works well for separate charged multiplicities, except for zero- and two-prong events. However, as noted before, if the zero- and two-prong events are combined, then the subtraction method becomes generally valid.

In Fig. 11, we show differential cross sections, and also the annihilation/ $(\bar{p}p - pp)$  ratio, for  $\gamma$  production as a function of  $x$ ,  $y^*$ , and  $p_T^2$ . Within the fairly large statistical errors we see much the same effects as for  $\pi^\pm$  production, i.e., broader distributions for the annihilations, and general agreement between  $\bar{p}p$  annihilations and  $(\bar{p}p - pp)$  differences.

It is commonly assumed that virtually all  $\gamma$ 's originate from  $\pi^0$  decays, and thus that  $\pi^0$  cross sections equal about half the photon cross sections. We have tried to use events with two-photon conversions detected to check this. Figure 12 shows the  $\gamma\gamma$  effective-mass spectrum in  $\bar{p}p$ . A clear  $\pi^0$  peak is seen, but no signal at the  $\eta$  meson;  $\eta$  production is clearly contributing  $\lesssim 10\%$  of the observed  $\gamma$ 's. In order to derive a  $\pi^0$  cross section, it is necessary to make a further correction. If a  $\pi^0$  decayed to two photons, one having energy  $< 120$  MeV in the laboratory, and the other below 120 MeV after c.m. reflection, then it would be completely lost from Fig. 12 because of our cuts. A Monte Carlo calculation

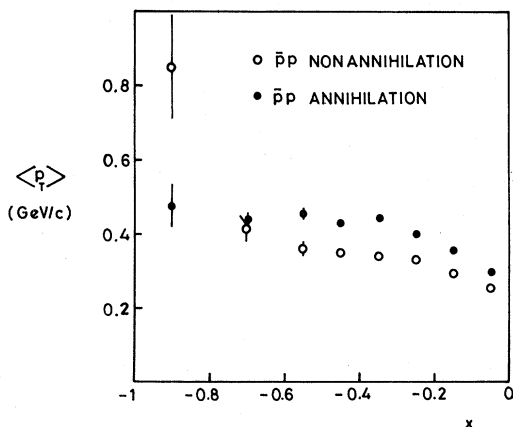


FIG. 10. Average transverse momentum of pions produced in  $\bar{p}p$  annihilations and nonannihilations, as a function of  $x$ .

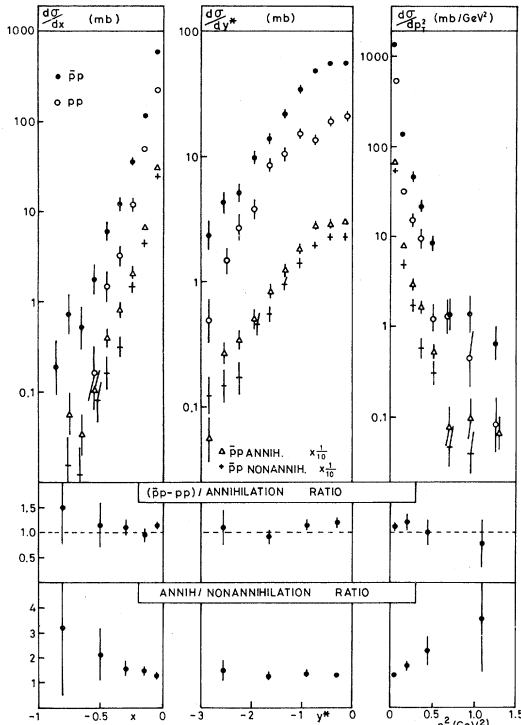


FIG. 11.  $d\sigma/dx$ ,  $d\sigma/dy^*$ , and  $d\sigma/dp_T^2$  for photon production. For clarity the  $\bar{p}p$  annihilation and nonannihilation data are scaled down by  $\frac{1}{10}$ . We also show  $(\bar{p}p - pp)/\text{annihilation}$  and annihilation/nonannihilation ratios.

was performed to calculate this effect. The  $\pi^0$  cross sections derived from the  $\gamma\gamma$  mass distributions were  $62 \pm 22$  mb for  $\bar{p}p$  and  $28 \pm 16$  mb for  $pp$ . These are certainly consistent with the whole contribution to the  $\gamma$  cross sections in Table X coming from  $\pi^0$  decays.

As a further test of this conjecture, it is plausible that, averaging over a large number of channels (in particular, averaging over all charged multiplicities),

$$\sigma(\pi^0) \simeq \frac{1}{2} [\sigma(\pi^+) + \sigma(\pi^-)]. \quad (1)$$

If this equation is correct, and if all  $\gamma$  rays come from  $\pi^0$  decays, then the  $\gamma$ -ray cross sections in Table X should equal the  $\pi^\pm$  cross sections of Table VIII. This appears to be true for  $pp$  interactions, but in  $\bar{p}p$  the  $\gamma$  cross sections are  $\sim 10\%$  higher in both annihilations and nonannihilations. Which of our two assumptions is incorrect is, however, not clear. It seems implausible that there should be a significant source of photons in  $\bar{p}p$  nonannihilations which is absent in  $pp$ . It is therefore likely that the  $\pi^0$  cross section is greater than indicated by Eq. (1) in the  $\bar{p}p$  case.

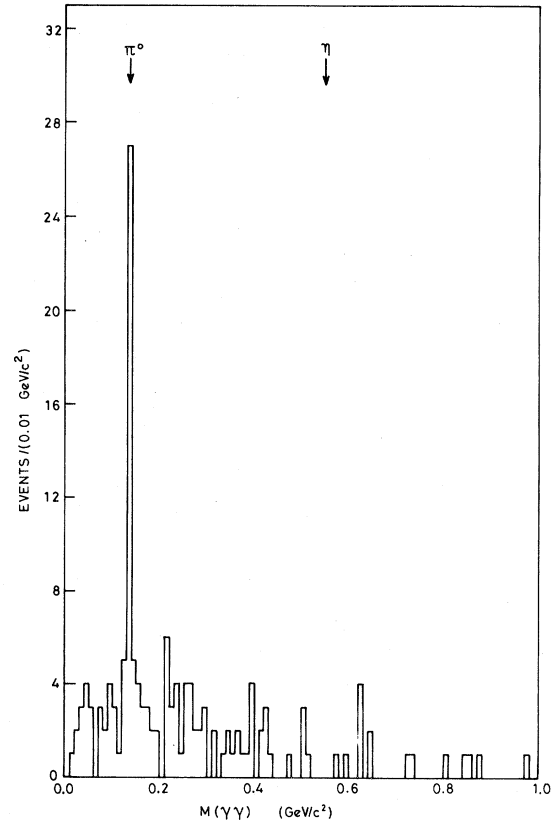


FIG. 12. Effective-mass distribution of  $\gamma\gamma$  pairs in  $\bar{p}p$  interactions.

#### D. Strange-particle production

As described in Sec. II,  $\Lambda^0$ ,  $\bar{\Lambda}^0$ , and  $K_S^0$  decays were identified by kinematic fitting, together with kinematic cuts to resolve the few ambiguities. To derive cross sections the data were weighted for scanning and measuring efficiencies, for decays closer than 1 cm to the production point or outside a fiducial volume and for neutral decay modes. Table XI gives our cross sections for  $K_S^0$  production, and Table XII for  $\Lambda^0/\bar{\Lambda}^0$  production. We have combined  $\Lambda^0$  and  $\bar{\Lambda}^0$  data (denoted by  $\Lambda/\bar{\Lambda}$ ) because their production cross sections are equal in  $\bar{p}p$ , and we would expect the forward production of  $\Lambda K$  in  $\bar{p}p$  to be similar to the forward production of  $\bar{\Lambda} K$  in  $pp$ . There were in fact no  $\bar{\Lambda}^0$  decays in the  $pp$  sample. Table XIII presents cross sections for the production of pairs of strange particles.

Some extra corrections were needed in order to obtain the annihilation cross sections shown in Tables XI–XIII. Events containing  $K_S^0$  in  $\bar{p}p$  interactions showed a larger number of neutral hadrons in the calorimeter than in  $pp$ . A large part of this excess could be attributed to associated  $K_L^0$ 's in-

TABLE X. Cross sections for photon production (in mb).

Charged multiplicity			$\bar{p}p$		$(\bar{p}p - pp)$
	$pp$	$\bar{p}p$	nonannihilation	annihilation	
0		6.6 ± 0.9	3.7 ± 1.1	2.9 ± 1.0	6.6 ± 0.9
2	33.4 ± 1.9	39.0 ± 2.1	29.7 ± 1.8	9.3 ± 1.0	5.6 ± 2.8
4	21.0 ± 1.5	52.4 ± 2.4	24.6 ± 1.9	27.8 ± 1.7	31.4 ± 2.8
6	2.48 ± 0.48	36.1 ± 2.0	3.0 ± 2.0	33.1 ± 4.0	33.6 ± 2.0
8		6.0 ± 0.8		6.0 ± 0.8	6.0 ± 0.8
10		0.55 ± 0.21		0.55 ± 0.21	0.55 ± 0.21
12		0.08 ± 0.08		0.08 ± 0.08	0.08 ± 0.08
Total	56.9 ± 2.6	140.7 ± 4.6	61.1 ± 3.0	79.6 ± 4.5	83.8 ± 5.3

teracting in the calorimeter, and thus being called  $\bar{n}$ 's. This effect, which was negligible except for the  $K_S^0$  events, was corrected using the distribution of observed  $K_S^0$ . A further small correction was made for the possibility of an  $n(\bar{n})$  from a  $\Lambda(\bar{\Lambda})$  decay interacting in the calorimeter. Neutral decay modes of  $\Lambda/\bar{\Lambda}$  had already been corrected for, so the possibility of double counting had to be avoided.

We see from Table XI that there is a substantial ( $\sim 50\%$ ) difference between the cross sections for  $K_S^0$  production in  $pp$  and  $\bar{p}p$  nonannihilations. We are confident that this effect is not caused by any remaining particle identification problems. Indeed, to a large extent the discrepancy can be explicitly associated with differences in hyperon-kaon pair production, as shown by the cross sections for  $\Lambda/\bar{\Lambda}$  and  $K_S^0$  production in Table XIII. In consequence, the  $(\bar{p}p - pp)$  difference method overestimates the  $K_S^0$  annihilation cross section. However, because  $\bar{p}p$  annihilations constitute a large part of  $K_S^0$  production at this energy, this overestimation is not a large effect, being  $\sim 13\%$ . It is not clear whether this discrepancy would get bigger or smaller at higher energies.

It is commonly proposed that the total annihilation cross section into kaonic channels may be obtained by assuming that

$$\begin{aligned}\sigma_A(K^+K^- + \pi's) &\simeq \sigma_A(K^+\bar{K}^0 + \pi's) \\ &\simeq \sigma_A(K^0K^- + \pi's) \\ &\simeq \sigma_A(K^0\bar{K}^0 + \pi's).\end{aligned}$$

On this assumption the total kaonic annihilation cross section in this experiment is

$$\sigma_A(K\bar{K} + \pi's) = 2\sigma_A(K_S^0) = 2.84 \pm 0.16 \text{ mb},$$

i.e.,  $(20 \pm 1)\%$  of the total annihilation cross section. However, it has been observed in Ref. 24 that under the same assumptions the ratio  $\sigma_A(K_S^0)/\sigma_A(K_S^0K_S^0)$  should equal 8. In fact, most experiments obtain values for this ratio  $\sim 6-7$ . Our value is 6.8. This clearly casts some doubt on the kaonic annihilation cross sections. One possibility is the existence of a four-kaon cross section at  $\sim 5-10\%$  of the two-kaon rate. Our best guess is probably that the kaonic annihilation cross section quoted above is an overestimate by  $\sim 10\%$ . In any case, kaon production is a significant component in the annihilation process.

In Fig. 13, we show differential cross sections for  $K_S^0$  production, together with annihilation/ $(\bar{p}p - pp)$  and annihilation/nonannihilation ratios. The annihilation/ $(\bar{p}p - pp)$  ratio shows no significant variation with  $x$ ,  $y^*$  or  $p_T$ , being systematically a lit-

TABLE XI. Cross sections for  $K_S^0$  production (in mb).

Charged multiplicity			$\bar{p}p$		$(\bar{p}p - pp)$
	$pp$	$\bar{p}p$	nonannihilation	annihilation	
0		0.13 ± 0.02	0.10 ± 0.03	0.024 ± 0.020	0.13 ± 0.02
2	0.28 ± 0.03	0.69 ± 0.04	0.32 ± 0.35	0.37 ± 0.05	0.41 ± 0.5
4	0.13 ± 0.02	0.86 ± 0.05	0.16 ± 0.04	0.70 ± 0.05	0.73 ± 0.05
6	0.008 ± 0.005	0.34 ± 0.03	0.034 ± 0.018	0.31 ± 0.03	0.33 ± 0.03
8		0.021 ± 0.007	0.002 ± 0.002	0.019 ± 0.007	0.021 ± 0.007
Total	0.42 ± 0.04	2.03 ± 0.10	0.62 ± 0.08	1.42 ± 0.08	1.61 ± 0.11

TABLE XII. Cross sections for  $\Lambda^0/\bar{\Lambda}^0$  production (in mb).

Charged multiplicity	$pp$	$\bar{p}p$	$(\bar{p}p - pp)$
0		0.44 $\pm$ 0.04	0.44 $\pm$ 0.04
2	0.60 $\pm$ 0.05	1.04 $\pm$ 0.06	0.44 $\pm$ 0.08
4	0.22 $\pm$ 0.03	0.34 $\pm$ 0.02	0.12 $\pm$ 0.04
6	0.019 $\pm$ 0.007	0.032 $\pm$ 0.010	0.013 $\pm$ 0.012
8	0.003 $\pm$ 0.003	0.002 $\pm$ 0.002	-0.001 $\pm$ 0.004
Total	0.84 $\pm$ 0.06	1.86 $\pm$ 0.10	1.02 $\pm$ 0.12

tle above 1. The longitudinal distributions are again slightly broader for annihilations than nonannihilations, but there does not seem to be much difference in shape in the  $p_T$  distributions. This is borne out by the mean values of  $p_T$  given in Table IX.

Table XII shows that there is a large difference in  $\Lambda/\bar{\Lambda}$  production between  $pp$  and  $\bar{p}p$  interactions. This difference cannot be associated with annihilations. [It is, of course, conceivable that a massive meson could be produced in an annihilation, which subsequently decayed into  $\Lambda\bar{\Lambda}$ . One would not expect this to be a significant effect at our energy, though, and this is borne out by the facts that the differences are seen mostly in low-multiplicity events, and appear to be peripheral (Fig. 14).] There is, however, another kind of interaction which can occur in  $\bar{p}p$  and not in  $pp$ , namely the production of hyperon-anti-baryon pairs with no associated kaons or baryons. Table XIII shows that  $\Lambda\bar{\Lambda}$  pair production accounts for 0.6 mb out of the 1 mb difference between the  $\Lambda/\bar{\Lambda}$  cross sections in  $\bar{p}p$  and  $pp$ . Presumably other hyperon pairs, such as  $\Lambda\bar{\Sigma}^\pm$  or  $\bar{\Lambda}\Sigma^\pm$ , are also produced in  $\bar{p}p$ , and we have also seen differences in  $\Lambda/\bar{\Lambda}K_S^0$  production, which must account for the remaining discrepancy.

Figure 14 shows differential cross sections for  $\Lambda/\bar{\Lambda}$  production (in the  $\bar{p}p$   $x$  and  $y^*$  distributions we show  $\Lambda$  and  $\bar{\Lambda}$  separately and combined), and also  $\bar{p}p/pp$  ratios. We see that the difference between  $\bar{p}p$  and  $pp$  are strongly enhanced at large  $x$  and  $y^*$ . There are no significant differences in the shapes of the  $p_T$  distributions.

### E. $\rho^0$ and $f^0$ production

We have estimated cross sections for  $\rho^0(770)$  and  $f^0(1270)$  production by means of fits to the  $\pi^+\pi^-$  effective mass distribution. We have used three different background parametrizations.

(i) The mass distribution was fitted to the following form (following Ref. 25):

$$d\sigma/dm = [1 + \alpha\omega(m) + \beta\rho(m) + \gamma f(m)] \\ \times (m - m_0)^a \exp(b + cm + dm^2).$$

Here,  $\alpha$ ,  $\beta$ ,  $\gamma$ ,  $a$ ,  $b$ ,  $c$ , and  $d$  are free parameters, and  $m_0 = 2m_\pi$ . The function  $\omega(m)$  represents the  $\pi^+\pi^-$  mass spectrum expected from  $\omega^0$  decay,<sup>26</sup> and  $\rho(m)$  and  $f(m)$  are  $p$ -wave and  $d$ -wave Breit-Wigner functions, respectively. In principle, this method was capable of giving  $\omega^0$  cross sections, but we found the numbers of  $\omega$ 's produced by the fit were erratic and had large errors, so we just treated the  $\omega$  term as a useful part of the background parametrization. The fit was carried out over the mass range 0.34–2.0 GeV/ $c^2$ . A typical fit is shown in Fig. 15.

(ii) Following Ref. 27, we have tried fitting the mass distribution above 0.6 GeV/ $c^2$  only, thus excluding most of the  $\omega$ -decay contribution. We used the forms

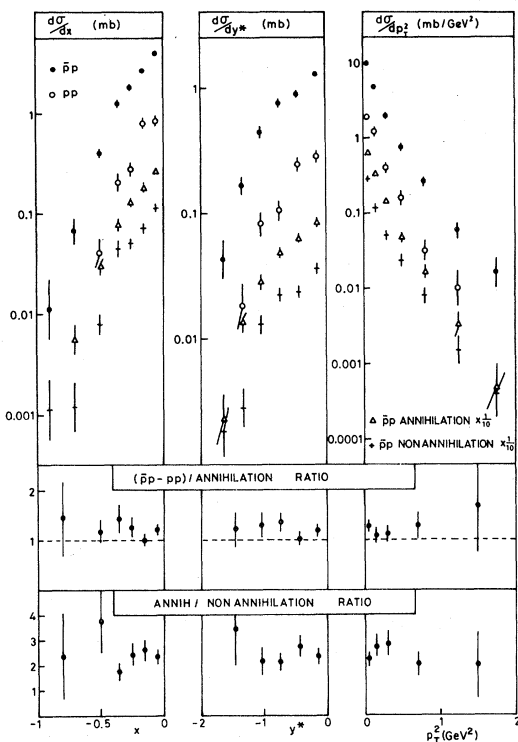
$$d\sigma/dm = [1 + \rho(m)] \exp(b + cm + dm^2),$$

$$0.6 < m < 1.0 \text{ GeV}/c^2, \text{ for } \rho^0$$

and

TABLE XIII. Cross sections for production of pairs of strange particles (in mb).

Channel	$pp$	$\bar{p}p$	$\bar{p}p$ nonannihilation	$\bar{p}p$ annihilation	$(\bar{p}p - pp)$
$K_S^0 K_S^0$	0.006 $\pm$ 0.006	0.23 $\pm$ 0.04	0.02 $\pm$ 0.01	0.21 $\pm$ 0.03	0.22 $\pm$ 0.04
$K_S^0 + \Lambda^0/\bar{\Lambda}^0$	0.12 $\pm$ 0.03	0.24 $\pm$ 0.04	0.24 $\pm$ 0.04		0.12 $\pm$ 0.05
$\Lambda^0 \bar{\Lambda}^0$		0.30 $\pm$ 0.05	0.30 $\pm$ 0.05		0.30 $\pm$ 0.05

FIG. 13. As Fig. 11 for  $K_S^0$  production.

$$d\sigma/dm = [1 + f(m)] \exp(b + cm + dm^2),$$

$$1.0 < m < 1.6 \text{ GeV}/c^2, \text{ for } f^0.$$

(iii) As an extension of method (ii) we fitted for  $\rho$  and  $f$  simultaneously over the mass range 0.6–1.5  $\text{GeV}/c^2$ , using a continuous background function over the whole range.

The fits generally gave consistent results for  $\rho^0$  production, but were not particularly consistent for  $f^0$  production. Our best estimates are obtained by averaging the results of the three fits, and appear in Table XIV. The cross sections are generally in agreement with Ref. 25 for  $\rho^0$  production, but we find significantly less  $f^0$  production. The data of Table XIV show that the  $(\bar{p}p - pp)$  differences are consistent with the annihilation cross sections, as our earlier results might lead us to expect for charge-conjugation eigenstates. In Table XIV, we also quote values for the  $\rho^0/\pi^-$  production ratios. This ratio measures the fraction of  $\pi^-$  originating from  $\rho^0$  decay, and is seen to be significantly higher in annihilations.

## V. COMPARISONS WITH QUARK MODELS

In the preceding section, we have compared several features of  $\bar{p}p$  annihilation and nonannihilation reactions. It is clear that most of the differ-

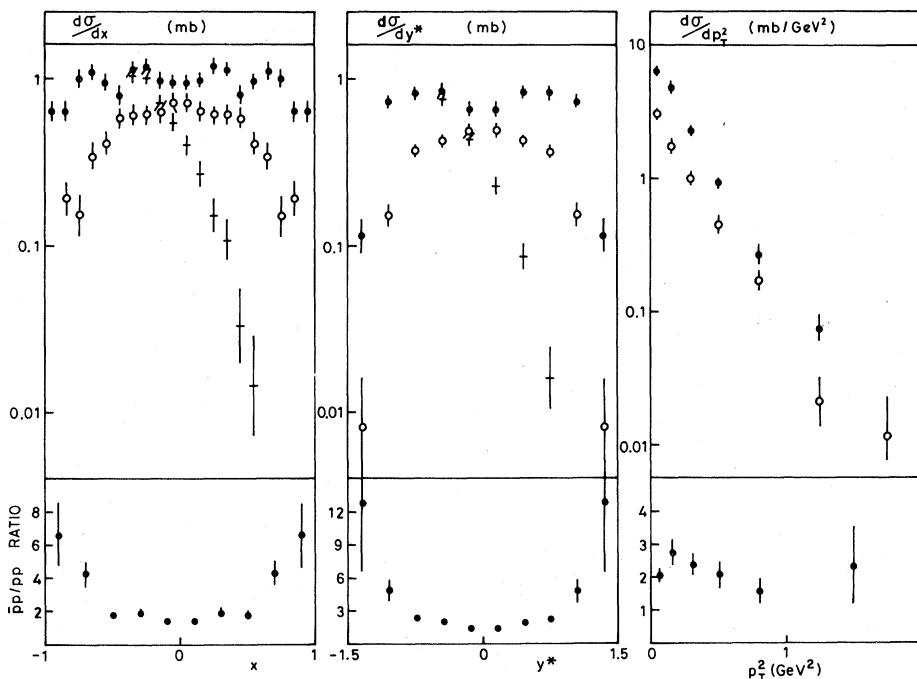


FIG. 14.  $d\sigma/dx$ ,  $d\sigma/dy^*$ , and  $d\sigma/dp_T^2$  for  $\Lambda/\bar{\Lambda}$  production. In the  $\bar{p}p$   $x$  and  $y^*$  distributions we also show data for  $\Lambda$  production alone where these data are significantly different from  $\Lambda/\bar{\Lambda}$  combined. We also show the ratio of  $\bar{p}p$  to  $pp$  cross sections.

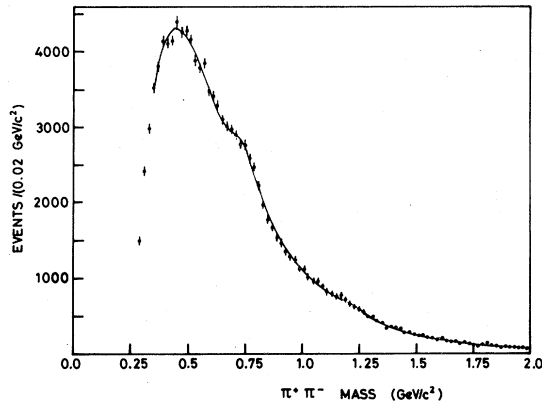


FIG. 15.  $\pi^+\pi^-$  effective-mass distribution in  $\bar{p}p$  interactions. A fit to background plus  $\omega$ ,  $\rho^0$ , and  $f^0$  production is superimposed.

ences seen can, at least in part, be accounted for as kinematic effects resulting from the baryon and antibaryon present in the nonannihilation reaction. One can then ask whether there is any difference in meson production between  $\bar{p}p$  annihilations and the central region of high-energy nonannihilations.<sup>8</sup> A model has recently been proposed using low-energy

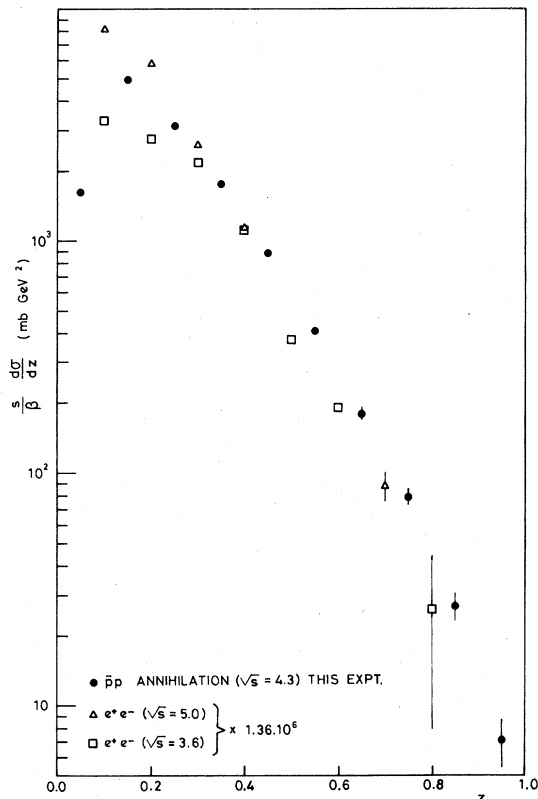


FIG. 16. Comparison between pion production in  $\bar{p}p$  annihilations and  $e^+e^-$  hadronic final states.

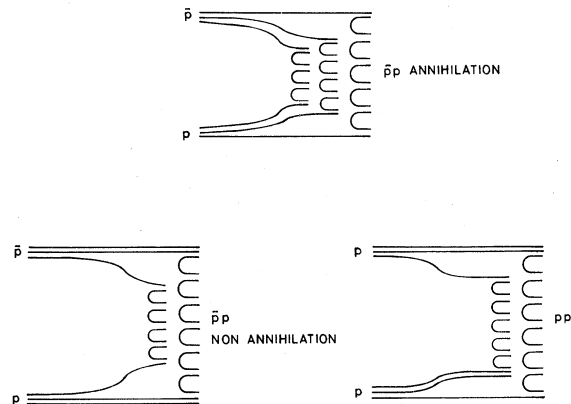


FIG. 17. Quark diagrams contributing to pion production in  $\bar{p}p$  and  $pp$  interactions.

annihilation data to predict high-energy  $pp$  cross sections using this idea.<sup>28</sup> A similar parallel has been drawn between  $e^+e^-$  annihilations into hadrons and central meson production in  $pp$  interactions at ISR energies.<sup>29</sup> It has also long been known that there are a number of remarkable similarities between  $\bar{p}p$  and  $e^+e^-$  annihilations into mesons (e.g., Ref. 30). For example, in Fig. 16 we compare our data with  $e^+e^-$  data in terms of the scaling cross section  $(s/\beta)d\sigma/dz$ , where  $z=2E^*/\sqrt{s}$  and  $\beta$  is the c.m. velocity of the produced particle. The normalization constant applied to the  $e^+e^-$  data is taken from Ref. 31. We see that the data agree well for  $z \geq 0.2$ .

Are we therefore to conclude that the mechanism of meson production is the same in all these reactions? This seems improbable, the production of a single  $q\bar{q}$  pair in a  $J^P=1^-$  state from a virtual photon in  $e^+e^-$  annihilations would appear to be much simpler than any process occurring in  $\bar{p}p$  annihilations. It seems likely that the dynamical similarities between  $e^+e^-$ ,  $\bar{p}p$  annihilations and nonannihilations reside in the limiting of transverse momentum to a common value of  $\sim 0.35$  GeV/c in each case. Phase-space effects may then explain most of the other similarities observed in, for example,  $x$  and  $y^*$  distributions, strange-particle yields, etc. This suggests that features like average multiplicities or longitudinal and transverse momentum distributions may not be sensitive ways of studying the  $\bar{p}p$  annihilation mechanism.

A more profitable approach may be to examine the leading-charge effects seen in annihilations. Although there is no leading-particle effect comparable to the large momentum given to the baryons in nonannihilation reactions, there is nevertheless a clear tendency for  $\pi^-$  ( $\pi^+$ ) to follow the direction

of the  $\bar{p}$  ( $p$ ) in  $\bar{p}p$  annihilations (see, for example, Fig. 8 or Ref. 11). This effect cannot be naturally explained in statistical models of annihilations, but lends itself to explanation in a quark model, if we suppose that the leading pions in annihilations contain valence quarks of the  $p$  and  $\bar{p}$ . We shall briefly consider two quark models, based on quark fragmentation and quark recombination.

The production of mesons in  $\bar{p}p$  annihilations and nonannihilations and  $pp$  interactions may be represented by the quark diagrams of Fig. 17. It has been suggested<sup>32,33</sup> that these diagrams may be interpreted in terms of an initial interaction which knocks the incident hadrons into colored constituents (three quarks and antiquarks in annihilations, quarks and diquarks in the nonannihilations), which subsequently "fragment" into hadrons as they separate in a similar way to  $e^+e^- \rightarrow$  hadrons or deep-inelastic scattering (DIS). If the momentum distributions of the fragmenting constituents are known the model can be calculated using fragmentation functions measured in  $e^+e^-$  or DIS.

However, if one naively uses the quark momentum distributions measured in DIS, this mechanism gives far too few mesons at large  $x$  or  $y^*$ .<sup>34</sup> The prescription proposed by the authors of Ref. 32 is that in the nonannihilation case one of the quarks carries a momentum as measured in DIS, and that the diquark effectively carries all of the remaining momentum. Analogously, Ref. 33 supposes that in the  $\bar{p}p$  annihilation case two quarks come from the DIS distributions, while the third carries all the remaining momentum. In Fig. 18, we compare our data on  $\pi^\pm$  production in  $\bar{p}p$  annihilations, nonannihilations, and  $pp$  interactions with the predictions of this model.

We see that the model can reproduce the data

quite well in the annihilation case. However, the agreement is poor for the  $pp$  and  $\bar{p}p$  nonannihilation data. The model has, however, been shown to work satisfactorily at higher energies for  $pp$  interactions, so possibly our energy is too low for the model to be applicable. However, the failure of the nonannihilation model suggests that the agreement with the annihilation data could be fortuitous. We note that the prescription for the quark distributions given in Ref. 33 corresponds to two of the quarks being held back near  $x=0$  (since the DIS quark distributions peak near  $x=0$ ), and the third quark and antiquark carrying off most of the momentum, and thus contributing most of the produced particles. This could provide some explanation of the similarity noted above between  $\bar{p}p$  and  $e^+e^-$  annihilations. We also note that in the nonannihilation model the diquarks carry off most of the momentum of the incident particles. Hence the diagrams of Fig. 17 indicate that different rapidity distributions may be expected for  $\bar{p}p$  nonannihilations and  $pp$ : in  $\bar{p}p$  we have a long ( $qq\bar{q}\bar{q}$ ) and a short ( $q\bar{q}$ ) chain, while in  $pp$  there are two similar ( $qq\bar{q}$ ) overlapping chains. This results in a narrower and higher rapidity distribution in  $\bar{p}p$  nonannihilations than in  $pp$ , as shown by the model curves in Fig. 18. We might hope to see at least a qualitative effect of this type in the data, but no significant differences at all are shown in the data.

The quark-recombination mechanism was put forward as a means of overcoming the failure of the naive quark-fragmentation model.<sup>34</sup> The idea is that the initial interaction principally affects the sea quarks, and that the valence quarks' momenta are largely unaltered by the collision. A high- $x$  meson may then be formed by a valence quark or antiquark picking up an antiquark or quark near

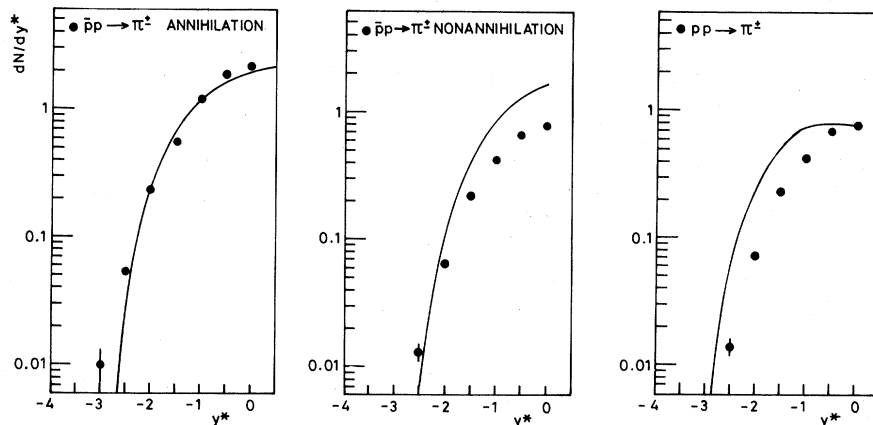


FIG. 18. Comparison of pion production in  $pp$  interactions,  $\bar{p}p$  nonannihilations, and annihilations with the quark-fragmentation model of Refs. 32 and 33.

TABLE XIV. Cross sections for  $\rho^0$  and  $f^0$  production (in mb).

	$\rho^0$	$f^0$	Ratio $\rho^0/\pi^-$
$pp$	$1.5 \pm 0.2$	$0.2 \pm 0.1$	$0.09 \pm 0.01$
$\bar{p}p$	$6.4 \pm 0.7$	$0.9 \pm 0.6$	$0.10 \pm 0.01$
$\bar{p}p$ nonannihilation	$1.9 \pm 0.3$	$0.2 \pm 0.1$	$0.07 \pm 0.01$
$\bar{p}p$ annihilation	$4.5 \pm 0.5$	$0.8 \pm 0.4$	$0.13 \pm 0.01$
$(\bar{p}p - pp)$	$4.9 \pm 0.7$	$0.7 \pm 0.6$	

$x=0$ . The  $x$  distribution of mesons at large  $x$  therefore closely resembles the momentum spectrum of the appropriate constituents inside the hadron, i.e.,  $\sim(1-x)^{3-4}$  for  $pp \rightarrow \pi^\pm$ .<sup>35</sup>

So can such a mechanism contribute to  $\bar{p}p$  annihilations? We have shown in Fig. 9 that the  $x$  distribution for pions is broader in annihilations than in nonannihilations. This can only be explained in the recombination picture if some of the valence quarks in an annihilation event have larger momentum fractions than in nonannihilations. For example, it is plausible to suppose that an annihilation is more likely to occur if one or more valence quarks from the proton combine with valence antiquarks from the  $\bar{p}$  to form low-mass mesons or gluons. [It is, of course, not inevitable that such a fusion of valence  $q$  and  $\bar{q}$  will lead to the destruction of the initial baryon number, i.e., annihilation. Indeed, a similar process is possible for many meson-proton interactions and appears to have a significant effect on meson production in the proton fragmentation region (Ref. 36). However, the valence  $q$ - $\bar{q}$  fusion process is present in  $\bar{p}p$  and not  $pp$  interactions, and since we have argued that  $(\bar{p}p - pp)$  differences are dominated by annihilations, it seems reasonable to associate this mechanism with initiating an annihilation.] The valence quark and antiquark which fuse will tend to have low  $x$  values, thus the remaining valence quarks will have larger momentum fractions on average. As an estimate of the size of the effect, assume one valence  $q$ - $\bar{q}$  pair near  $x=0$  fuses: from dimensional-counting arguments,<sup>37</sup> we expect the remaining valence quarks to have an  $x$  dependence like  $(1-x)$ , compared to  $(1-x)^3$  if no fusion took place. We may thus expect the  $(1-x)^n$  dependence of pion production in annihilations to differ from nonannihilations by  $\sim 2$  units in the exponent  $n$ .

In Fig. 19, we show our data on  $\pi^\pm$  production plotted against  $(1-|x|)$ , for annihilations and nonannihilations. The observed exponents of  $(1-x)$  are 1.9 and 3.5, respectively. These are both somewhat larger than the simple values expected from dimensional counting, namely 1 and 3. Part of this may be caused by the presence of indirectly produced

pions (from resonance decays) in the data. Also, assuming the fusing quarks in the annihilation case had  $x=0$  was not quite correct; Ref. 38 attempts to allow for the kinematic effects of these quarks, and obtains an exponent of 1.5.

We make a final comment on the recombination model in connection with the  $\pi^-/\pi^+$  ratios of Fig. 8. According to the recombination model, the  $\pi^-/\pi^+$  ratio should equal the valence  $d/u$  quark ratio at large  $x$ . We see a significantly higher  $\pi^-/\pi^+$  ratio in annihilations than nonannihilations. This can be understood if the initial  $q$ - $\bar{q}$  fusion mechanism in  $\bar{p}p$  annihilations forms isoscalar mesons or gluons to a significant extent. In this case  $u\bar{u}$  fusion will be four times more likely than  $d\bar{d}$  fusion, and the  $d/u$  ratio of the remaining valence quarks enhanced. However, it must be noted that Fig. 8 does show significant differences between the  $\pi^-/\pi^+$  ratios in  $\bar{p}p$  nonannihilations and  $pp$  interactions, though not so great as the differences between annihilations and nonannihilations. This shows that the simple recombination picture presented here is not the whole story, very possibly the  $q$ - $\bar{q}$  fusion mechanism also makes some small contribution to  $\bar{p}p$  nonannihilations.

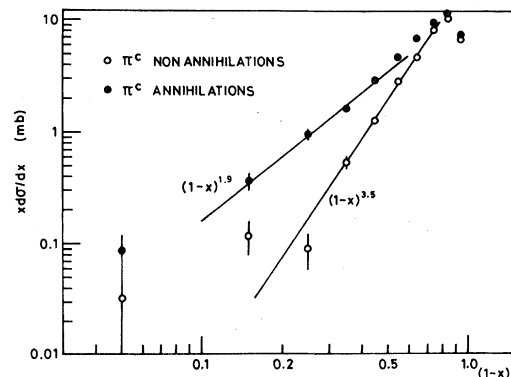


FIG. 19.  $x d\sigma/dx$  plotted against  $(1-|x|)$  for pion production in  $\bar{p}p$  annihilations and nonannihilations, together with power-law fits to the large- $x$  data.

## VI. SUMMARY

We have studied a number of aspects of  $\bar{p}p$  annihilations at 8.8 GeV/c, with particular emphasis on the  $(\bar{p}p - pp)$  difference technique as a means of deriving annihilation data. Our main conclusions are as follows.

(i) For topological cross sections the  $(\bar{p}p - pp)$  difference method is satisfactory for  $\geq$  four-prong events. If zero- and two-prong events are combined, then again the difference method works, or alternatively the "corrected difference" procedure of Ref. 5 may be adopted. It seems likely that the  $(\bar{p}p - pp)$  technique will continue to be reliable at higher energies.

(ii) We find that  $(\bar{p}p - pp)$  differences give a good description of pion production in  $\bar{p}p$  annihilations, provided  $\pi^+$  and  $\pi^-$  are combined. The only exception is possibly at large  $p_T$ . Considering  $\pi^+$  and  $\pi^-$  separately, we find discrepancies between  $(\bar{p}p - pp)$  and annihilations of  $\sim 10\%$  in the proton fragmentation region, rising to  $\sim 20\%$  in the central region of phase space.

(iii) In the case of photon production,  $(\bar{p}p - pp)$  differences agree well with annihilations. We see no evidence for any source of photons other than  $\pi^0$  decays. It does appear that  $\pi^0$ 's are more copiously produced (compared to  $\pi^\pm$ ) in  $\bar{p}p$  interactions (both annihilation and nonannihilations) than in  $pp$  interactions.

(iv) It appears that  $(\bar{p}p - pp)$  differences slightly overestimate the production of  $K_S^0$  in annihilations. There are large differences in  $\Lambda/\bar{\Lambda}$  production between  $\bar{p}p$  and  $pp$ , associated with peripheral  $\Lambda\bar{\Lambda}$  pair production in  $\bar{p}p$ .

(v) We have compared our pion-production data with two quark models. The quark-fragmentation model of Refs. 32 and 33 is successful in describing the annihilation data, but fails badly for  $\bar{p}p$  nonannihilation and  $pp$ . To apply the quark-recombination model to the  $\bar{p}p$  annihilation process, we need to assume that at least one pair of valence quark and antiquark annihilates near  $x=0$  to initiate the interaction. In this case the recombination picture gives a satisfactory qualitative explanation of the data.

## ACKNOWLEDGMENTS

We would like to thank SLAC and SHF personnel for their assistance during the running of this experiment, and to thank our scanning and measuring staff for their outstanding efforts. D.R.W. and C.N.B. acknowledge financial support from Laser-Scan Limited, Cambridge. This research was supported in part by the U. K. Science and Engineering Research Council and by the U. S. National Science Foundation.

\*Present address: Bell Telephone Laboratories, Columbus, Ohio.

<sup>1</sup>H. Muirhead, in *Proceedings of the II European  $\bar{N}N$  Symposium, Liblice-Prague, 1974*, edited by L. Montanet (CERN, Geneva, 1974), p. 488. See also Ref. 6.

<sup>2</sup>P. Gregory *et al.*, Nucl. Phys. **B119**, 60 (1979).

<sup>3</sup>P. Johnson *et al.*, Nucl. Phys. **B173**, 77 (1980).

<sup>4</sup>J. G. Rushbrooke *et al.*, Phys. Lett. **59B**, 303 (1975).

<sup>5</sup>R. M. Robertson *et al.*, Phys. Rev. D **21**, 3064 (1980).

<sup>6</sup>J. G. Rushbrooke and B. R. Webber, Phys. Rep. **44C**, 1 (1978).

<sup>7</sup>R. A. Lewis *et al.*, in *Proceedings of the IV European Antiproton Symposium, Barr*, edited by A. Fridman (Editions du Centre National de la Recherche Scientifique, Paris, 1979), Vol. II, p. 209.

<sup>8</sup>D. R. Ward, in *Proceedings of the Fifth European Symposium on Nucleon-Antinucleon Interactions, Bresanone, Italy, 1980* (Istituto Nazionale Fisica Nucleare, Padua, 1980), p. 459.

<sup>9</sup>M. Pratap *et al.*, Phys. Rev. D **19**, 1955 (1979).

<sup>10</sup>A. J. Simmons *et al.*, Nucl. Phys. **B172**, 285 (1980).

<sup>11</sup>D. R. Ward *et al.*, Nucl. Phys. **B172**, 302 (1980).

<sup>12</sup>J. Ballam and R. D. Watt, Annu. Rev. Nucl. Sci. **27**, 75 (1977).

<sup>13</sup>A. J. Simmons, Ph.D. thesis, Cambridge University, 1979 (unpublished).

<sup>14</sup>C. P. Ward *et al.*, Nucl. Phys. **B153**, 299 (1979).

<sup>15</sup>C. N. Booth, Ph.D. thesis, Cambridge University, 1981 (unpublished).

<sup>16</sup>V. Flaminio *et al.*, Report No. CERN/HERA 79-03 (unpublished).

<sup>17</sup>A. D'Innocenzo *et al.*, Lett. Nuovo Cimento **28**, 369 (1980).

<sup>18</sup>J. Whitmore, Phys. Rep. **27C**, 187 (1976).

<sup>19</sup>R. Raja, Phys. Rev. D **16**, 142 (1977).

<sup>20</sup>C. Bromberg *et al.*, Nucl. Phys. **B107**, 82 (1976).

<sup>21</sup>D. Everett *et al.*, Nucl. Phys. **B73**, 440 (1974).

<sup>22</sup>T. Knasel *et al.*, DESY Report No. 70/3, 1970 (unpublished).

<sup>23</sup>D. R. Ward, UA5 Internal Report No. CERN/EP/SCE-R703T-UA5/570-2 (unpublished), based on the method in S. Jadach, Comput. Phys. Commun. **9**, 297 (1975).

<sup>24</sup>G. D. Patel, in *Proceedings of the Fifth Symposium on*

- Nucleon-Antinucleon Interactions, Bressanone, Italy, 1980* (Ref. 8), p. 119.
- <sup>25</sup>M. Markytan *et al.*, Nucl. Phys. **B143**, 263 (1978).
- <sup>26</sup>H. Pilkuhn, *The Interactions of Hadrons* (North-Holland, Amsterdam, 1967), p. 143.
- <sup>27</sup>V. Karimaki *et al.*, Z. Phys. C **9**, 117 (1981).
- <sup>28</sup>A. D'Innocenzo *et al.*, Lett. Nuovo Cimento **27**, 457 (1980); A. D'Innocenzo *et al.*, in *Proceedings of the Fifth European Symposium on Nucleon-Antinucleon Interactions, Bressanone, Italy, 1980* (Ref. 8), p. 383.
- <sup>29</sup>M. Basile *et al.*, Phys. Lett. **92B**, 369 (1980).
- <sup>30</sup>H. Muirhead, in *Proceedings of the International Symposium on  $\bar{p}p$  Interactions, Loma-Koli, Finland, 1975*, edited by J. Tuoriniemi (University of Helsinki, Helsinki, 1975), p. 300.
- <sup>31</sup>C. A. Nelson, Lett. Nuovo Cimento **11**, 517 (1974).
- <sup>32</sup>A. Capella *et al.*, Z. Phys. C **3**, 329 (1980).
- <sup>33</sup>U. Sukhatme *et al.*, Phys. Rev. Lett. **45**, 5 (1980).
- <sup>34</sup>K. P. Das and R. Hwa, Phys. Lett. **68B**, 459 (1977).
- <sup>35</sup>W. Ochs, Nucl. Phys. **B118**, 397 (1977).
- <sup>36</sup>B. Buschbeck *et al.*, Z. Phys. C **7**, 73 (1980).
- <sup>37</sup>S. Brodsky and J. Gunion, Phys. Rev. D **17**, 1788 (1978).
- <sup>38</sup>H. Muirhead *et al.*, Z. Phys. C **9**, 87 (1981).